BRIGHAM YOUNG UNIVERSITY

# GEOLOGY STUDIES

VOLUME 40 • 1994

# BRIGHAM YOUNG UNIVERSITY GEOLOGY STUDIES

Volume 40, 1994

CONTENTS

A Publication of the
Department of Geology
Brigham Young University
Provo, Utah 84602



*Brigham Young University Geology Studies* is published by the Department of Geology. This publication consists of graduate student and faculty research within the department as well as papers submitted by outside contributors. Each article submitted is externally reviewed by at least two qualified persons.

ISSN 0068-1016
6-94 550 10461/11134

# Geology and Geochemistry of the Golden Butte Mine—A Small Carlin-Type Gold Deposit in Eastern Nevada

DAVID J. WILSON
ERIC H CHRISTIANSEN
DAVID G. TINGEY

*Department of Geology, Brigham Young University, Provo, Utah 84602*

ABSTRACT

The Golden Butte sediment-hosted disseminated (Carlin-type) gold deposit is located on the western flank of the Cherry Creek Range in east central Nevada. The ore body contains nearly 3 million tons of gold ore with an average grade of 0.031 ounces per ton. The main host of the gold ore is the Mississippian Chainman Shale, a carbonaceous, silty claystone to siltstone. A low-angle (normal?) fault has superimposed Chainman Shale over unmineralized Devonian Simonson Dolomite. A second low-angle fault has placed the Simonson Dolomite over Chainman Shale. Two high-angle, basin-and-range-style faults cut the low-angle faults and served as conduits for ascending hydrothermal fluids. Solution by hydrothermal fluids and repeated movement on both sets of faults before and during mineralization created highly permeable pathways and many bodies of breccia.

Hydrothermal alteration of the Chainman Shale included removal of carbonate, silicification (jasperoid), argillization, and dolomitization. Gold mineralization is found in all alteration types, but jasperoid is the most important host for ore. Jasperoid is commonly brecciated, and vugs and veins indicate multiple stages of silicification. Minerals associated with the jasperoid include coarsely crystalline quartz, stibnite, pyrite, and local cinnabar and realgar. Oxidized zones and veins cut across other alteration types and include late-formed stibiconite, barite, calcite, limonite, and hematite. Alteration in the Simonson Dolomite is less extensive and includes jasperoid, argillic, sanded dolomite, and late oxidized types.

Major-element analyses show the jasperoid at Golden Butte is similar to other jasperoids related to Carlin-type deposits. Isocon diagrams reveal that Au, Ag, As, Sb, Hg, Tl, Sc, and Th are significantly enriched in the alteration products. Volume increases (locally as much as 400%) during alteration, especially for the ore-hosting jasperoid, where up to 500% $SiO_2$ was introduced, were important. The change in volume occurred by filling of open spaces in a porous, repeatedly brecciated host. Principal component analysis of the geochemical data partitioned most of the pathfinder elements in a factor separate from Au and Ag in all alteration types. This suggests that precious-metal mineralization may have occurred separate in space and/or time from the event that deposited most of the pathfinder elements or that there were differing solubilities of the elements in the hydrothermal solutions. For jasperoid samples, another factor may be related to residual immobile elements and argillic components.

Fluid inclusions suitable for microthermometry are rare. However, inclusions found in jasperoid and vein quartz, vein barite, and late calcite are uniformly liquid-rich and $CO_2$-poor; no evidence for boiling of the hydrothermal fluids was found. Homogenization temperatures of inclusions in jasperoid quartz ranged between 180° and 295°C, with salinities between 4.5 and 6 equiv wt percent NaCl. Inclusions in quartz veins had homogenization temperatures from 135° to 200°C and salinities of 4.5 to 6 equiv wt percent NaCl. Inclusions in late barite and calcite veins had low salinities (< 2 equiv wt% NaCl). Accurate homogenization temperatures could not be obtained from inclusions in barite due to stretching of the fluid inclusions.

The sequence of events believed to have produced the mineralization at Golden Butte was (1) post-Paleozoic, low-angle faulting; (2) late Cenozoic high-angle faulting and associated brecciation; (3) wall-rock alteration and gold mineralization by the influx of hydrothermal fluids ascending along high-angle faults—fluids spread laterally into the Chainman Shale, silicifying it, removing Ca, Mg, and S, and depositing Au, Ag, As, Sb, Hg, and Tl; (4) continued solution and tectonic brecciation, alteration, and possible gold deposition; (5) late veining by cooler hypogene fluids; and (6) oxidation by supergene fluids and weathering. The jasperoids lack the trace element characteristics of porphyry-related deposits, and the deposit is probably related to deep circulation of fluids initiated by high-angle faulting.

## INTRODUCTION

Over the last 25 years sediment-hosted disseminated (Carlin-type) gold deposits have become important sources of gold in the United States. Many deposits of this type have been discovered in the Great Basin of Nevada and Utah. The most well known is the Carlin Mine in north central Nevada. Carlin-type deposits are typified by (1) micron- to submicron-size gold particles dispersed more or less uniformly throughout the ore; (2) carbonate or silty carbonate host rocks; (3) hydrothermal alteration that includes removal of carbonate along with silicification, dolomitization, argillization, and carbonization; (4) gold ore localized in areas of high-angle faults, thrust faults, and brecciated rock; (5) high concentrations of Au, Ag, As, Sb, Ba, Tl, and Hg and low concentrations of Cu, Pb, and Zn in the altered rocks; and (6) late crosscutting veins of quartz, barite, and calcite (Radtke and Dickson 1974, Tooker 1985). Sediment-hosted gold deposits contain between 1 and 24 million tons, with 50% of the deposits having tonnages greater than 5.1 million tons. Ore grades range between 0.024 and 0.27 ounces per ton (0.84 to 9.2 ppm), with 50% of the deposits having a grade of 0.088 ounces per ton (3 ppm) or more (Berger 1986). The Carlin deposit consists of more than 22 million tons of gold ore with a grade of 0.3 ounces per ton (10 ppm) (Romberger 1986).

Uncertainties remain about the controls of stratigraphy and structure on Carlin-type mineralization, the extent and nature of metasomatism (including the origin of jasperoid), and the characteristics of the ore fluids. Consequently, we embarked on a study of the Golden Butte Mine, a marginally economic Carlin-type deposit in east central Nevada (fig. 1), where alteration and gold distribution have clear associations with structure and stratigraphy. Field, geochemical, petrographic, and fluid inclusion studies were used to document its characteristics and constrain some of the physical and chemical characteristics of the gold-carrying fluid and the products of its reaction with sedimentary wall rocks.

The study of small deposits like Golden Butte are important in elucidating the transition from subeconomic to economic mineralization. What geological and geochemical processes differentiate small low-grade deposits from large high-grade deposits? Are marginal deposits simply smaller versions of their larger relatives, or are critical features present in large deposits missing in small deposits? Answers to these questions can only be reached through studies of small deposits and will eventually help us focus our attention on the most important aspects of ore formation. Moreover, small deposits may, in some cases, display the critical features and defining reactions of a deposit type better than their larger and, oftentimes, more altered equivalents.

## METHODS OF STUDY

Geologic maps of the 6,865-foot and part of the 6,850-foot elevation levels of the pit were constructed at a scale of 1:600 using surveyed points, a compass, and measuring tape. Geologic maps, reports, gold assays, and drill logs completed earlier by the Alta Gold Company and previous owners of the property were also used.

Seventy-two samples were collected for geochemical and petrographic study, primarily from inside the pit. Samples of Simonson Dolomite (from 2 km southeast of the mine) and the ore-hosting Chainman Shale (from 1 km northeast of the mine) were collected in areas removed from the effects of alteration.

Thin plates, doubly polished to 0.1 mm thick, were examined for fluid inclusions on a Fluid Inc. gas-flow, heating and freezing stage mounted on a Zeiss microscope. The stage was calibrated using pure $H_2O$ (Tm = 0°C) and $CO_2$ (Tm = –56.6°C) in synthetic fluid inclusion standards; high temperatures were monitored by checking the melting points of tin (231.97°C), lead (327.43°C), and cadmium iodide (385°C). Repeat freezing point measurements had a reproducibility of about ±0.1°C; vapor-liquid homogenization temperatures were reproducible at ±1° to 2°C.

Samples were analyzed for Au, and 14 other trace elements (Cu, Zn, Ga, As, Se, Mo, Ag, Cd, Sb, Te, Au, Hg, Tl, Pb, Bi), commonly called pathfinders, by Geochemical Services Incorporated using inductively coupled plasma emission spectrometry. Samples (5 g) digested in a strong oxidizing acid mixture and selectively extracted into an

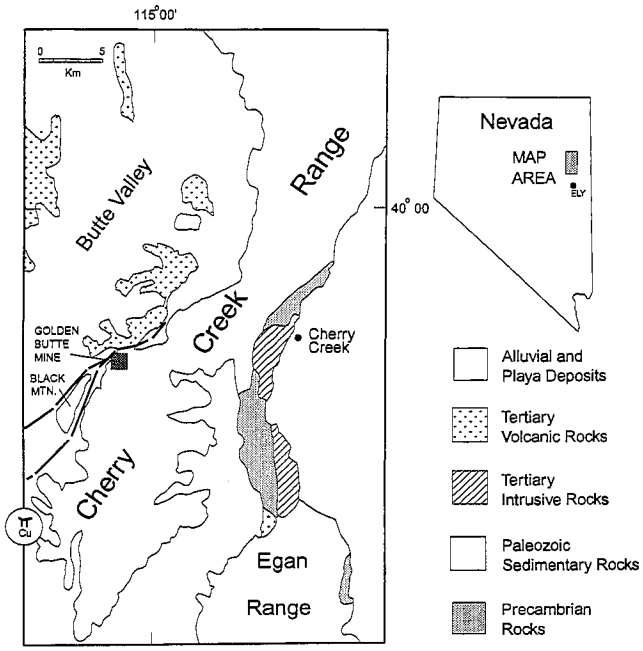


FIGURE 1.—*Generalized geologic map of the southern Cherry Creek and northern Egan Ranges, east central Nevada (Hose and Blake 1976). π Cu indicates approximate position of a buried porphyry system.*

organic solution. This method does not digest silicates completely, and the reported concentrations of Pb, Ga, and Tl are low because significant fractions of these elements reside in silicate minerals. Precision of the analyses was estimated by analyzing duplicates of three samples (Cu ±6%, Zn ±7%, As ±12%, Sb ±15%, Tl ±9%, Mo ±1 ppm, Ag ±0.01 ppm, Cd ±0.05 ppm, Au ±0.03 ppm, Hg ±0.4 ppm, Pb ±0.3 ppm). Major elements (Si, Ti, Al, Fe, Mn, Mg, Ca, K, P) were analyzed at Brigham Young University using a Phillips X-ray fluorescence (XRF) spectrometer on glass discs formed by fusing rock powder with lithium metaborate doped with lanthanum (Norrish and Hutton 1969). Concentrations of S, Sc, V, Ni, Cu, Zn, Ga, Rb, Sr, Y, Zr, Nb, Ba, La, Ce, Nd, Th, and $Na_2O$ were also determined by XRF using pressed powder pellets and mass absorption coefficients calculated from major-element analyses. Accuracy was assessed from multiple analyses of international geochemical reference standards (Rb, Sr, Y, Zr, Nb, V, Ni, Cu, Zn, Ga, Th ±1–2 ppm; Sc, Nd ±3 ppm; Ba, La, Ce ±6–9 ppm; $SiO_2$ ±0.2%, $Al_2O_3$, MgO ± 0.05–0.07%; $TiO_2$, MnO, CaO, $P_2O_5$ ±0.01–0.02%; $Fe_2O_3$, $K_2O$ ±0.03–0.04%; $Na_2O$ ±0.1% at one standard deviation). Zinc, Cu, and Ga were analyzed by both XRF and ICP methods. The concentrations of Ga (which is concentrated in silicates because it behaves like Al) analyzed by ICP and XRF are generally not in agreement because the ICP analysis represented only a partial digestion. Zinc and Cu concentrations agreed within a few percent of each other, demonstrating that these elements are present outside of silicates, probably as sulfides in the samples. Average compositions for the various rock types were calculated by removing anomalous values and arbitrarily assigning concentrations of 50% of the detection limit to analyses below the detection limit.

## GEOLOGY OF EAST CENTRAL NEVADA

From the late Proterozoic to the Early Triassic, what is now eastern Nevada was part of the Cordilleran miogeocline. During this period, approximately 9,000 to 12,000 m of sedimentary rock accumulated on a shallow, carbonate-dominated shelf formed on a rifted continental margin (Stewart 1980) underlain by Proterozoic igneous and metamorphic rocks. The sedimentary rocks consist primarily of quartzite, limestone, and dolomite with minor sandstone, siltstone, and shale. During the Paleozoic, mild regional upwarps caused depositional hiatuses in some sections. Eastern Nevada lay east of the late Devonian to early Pennsylvanian Antler orogenic belt and received detritus shed into a foreland basin that formed the late Devonian to early Mississippian Pilot Shale and Mississippian Chainman Shale (Hose and Blake 1976).

Middle to Upper Triassic and Jurassic sedimentary deposits are absent in east central Nevada. The only Cretaceous sedimentary rocks in the area are nonmarine strata in the Diamond Mountains and the Pancake Range 50 km southwest of the Cherry Creek Range. A series of Mesozoic to early Tertiary tectonic events, likely related to the Elko and Sevier orogenies, produced thrust faults and large amplitude folds (Thorman and others 1991). An arched area formed in the vicinity of the Schell Creek and northern Egan range that was bounded by broad synclines on the east (Confusion Range structural trough) and the west (Butte structural trough) (Hose and Blake 1976). The northern Egan and Cherry Creek Ranges (fig. 1), where the Golden Butte Mine is located, consist of west-dipping sedimentary units on the eastern flank of the Butte structural trough. These folds were eroded, covered partially by Tertiary volcanic rocks, further tilted to the west along basin-and-range faults, and eroded to their present configuration during the Tertiary (Smith 1976).

Intrusive rocks are present in nearly all of the ranges in eastern Nevada. Radiometric ages of these plutons range from approximately 160 to 32 Ma (Hose and Blake 1976). Two granitic plutons and many dikes are present in the northern Egan Range in the area of the old Cherry Creek mining district, approximately 15 km east of the Golden Butte Mine (fig. 1). A biotite granite 2 km west of the town of Cherry Creek has an average zircon and titanite fission

track age of 40 ± 4 Ma (Hose and Blake 1976). The age of a porphyritic biotite granite dike 10 km southwest of Cherry Creek has been determined, by the K-Ar method, to be 32.9 ± 0.6 Ma (Armstrong 1970; recalculated using new IUGS decay constants). No intrusions are exposed in the southern Cherry Creek Range. However, a buried subeconomic porphyry sulfide system, covering an area of less than 10 km$^2$, was discovered in 1969, using geophysical means, by the Bear Creek Mining Company (Miller 1971, Welsh and Miller 1990). This mineralized intrusion is on the east side of Butte Valley, only about 5 km southwest of the Golden Butte Mine (fig. 1).

Tertiary volcanic rocks and lesser sedimentary rocks are present throughout the ranges of eastern Nevada. The principal volcanic units consist of rhyolitic tuffs and andesitic to rhyolitic lava flows of probable middle Tertiary age (e.g., Gans and others 1989, Hose and Blake 1976).

The present north-trending ranges and valleys were formed during the late Cenozoic by extensional normal faulting similar to that in other areas of the Basin and Range Province. The role of middle Tertiary low-angle normal faulting, like that found by Gans and others (1989) in the Egan Range, is problematic in the Cherry Creek Range. Nonetheless, total Cenozoic extension across this region (southern Cherry Creek and northern Egan Ranges) was relatively minor, roughly 10% (Smith and others 1991)

## GOLDEN BUTTE DEPOSIT

The Golden Butte Mine is located on the western flank of the Cherry Creek Range about 15 km southwest of the town of Cherry Creek (fig. 1). The property consists of 355 claims that contain two defined ore bodies, Golden Butte and North Golden Butte. The mine was operated as a 60-40 joint venture between Alta Gold and Echo Bay, with Alta Gold as operator. The ore body was worked as an open pit mine, and the gold was extracted using standard heap leaching methods.

The Golden Butte ore body had an estimated 2,748,000 tons of minable ore with an average grade of 0.031 ounces of gold per ton (1.1 ppm) for a total of 84,500 ounces of contained gold; 64,000 ounces were recoverable. The North Golden Butte ore body has an estimated 60,000 ounces minable, but it is not currently economical to mine (N. A. Johnson written communication 1990).

## GEOLOGIC SETTING

### *Stratigraphy*

The oldest unit exposed in the mine area is the Devonian Simonson Dolomite. It is medium grayish brown, laminated, micritic to coarsely crystalline, and generally nonfossiliferous. Fossils in the mine area are poorly preserved and consist of crinoidal debris and horn corals. Such coarse-grained dolomite is characteristic of the lower member of the Simonson Dolomite (Osmond 1954). Inside the pit, the Simonson Dolomite is well bedded, with beds generally between 3 cm and 1 m thick, striking north 10° to 20° east and dipping 25° to 35° west (fig. 2). Locally, the dolomite has abundant joints that generally strike northeast and dip at high angles. The thickness of this formation in the Cherry Creek and northern Egan Ranges, as measured by Fritz (1968), is 400 m.

The Devonian Guilmette Formation conformably overlies the Simonson Dolomite and is exposed in the central part of the Cherry Creek Range 3 km south of the mine. This unit is composed of medium-bedded, dark brownish gray micritic limestone and is characteristically fossil rich with stromatoporoids, brachiopods, and corals most common (Hose and Blake 1976). The Guilmette Formation is 425 m thick in the Cherry Creek Range (Fritz 1968).

The late Devonian to early Mississippian Pilot Shale conformably overlies the Guilmette Formation south of the mine. This unit rarely crops out and typically forms covered slopes and hummocks. Generally, the Pilot Shale

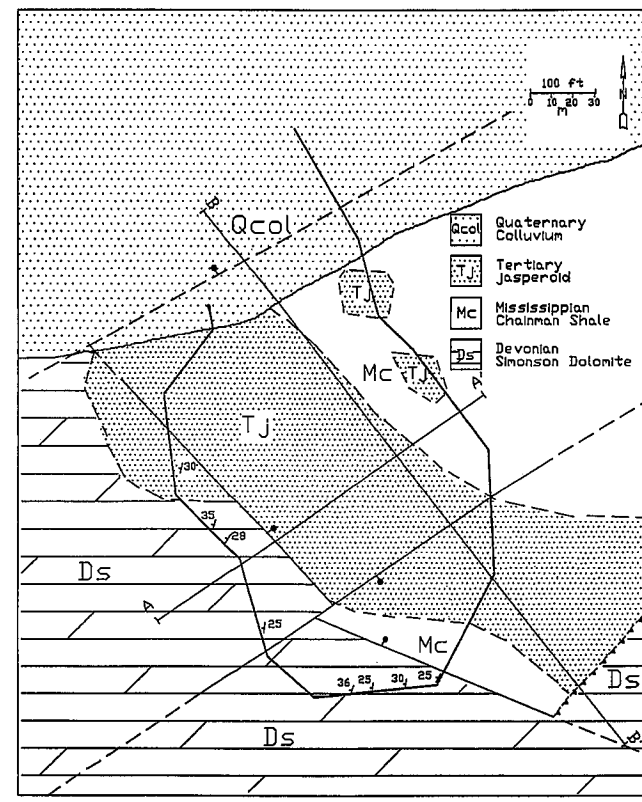


FIGURE 2.—*Geologic map of the 6,868-foot elevation level of the Golden Butte pit and surrounding area. The low-angle fault (marked with sawteeth on upper plate) is shown as seen in a plan view of the pit.*

is thinly laminated, dark gray, carbonaceous, calcareous siltstone and silty shale. The silty shales are generally dolomitic but are locally limy (Hose and Blake 1976). The total thickness of the Pilot Shale in the Cherry Creek Range is 190 m (Fritz 1968).

The Mississippian Joana Limestone conformably overlies Pilot Shale and consists of medium- to thickly bedded limestone. This unit is characteristically cherty, bioclastic, and is only 35 m thick in the Cherry Creek Range (Fritz 1968).

The Mississippian Chainman Shale, the main host rock for the gold ore at Golden Butte, is composed of carbonaceous, pyritic, silty to sandy claystone and siltstone. The dark, organic-rich, poorly exposed, incompetent beds are commonly severely deformed (Hose and Blake 1976). We do not know what portion of the Chainman Shale is exposed in the mine, but a thin limestone unit 8 m above the base of the Chainman Shale mapped by Fritz (1968) in the southern portion of the Cherry Creek Range does not appear to be present near the mine. Total thickness of this unit in the Cherry Creek Range is 310 m (Fritz 1968). The Chainman Shale is also the principal host for disseminated gold mineralization in the Nighthawk Ridge deposit at Easy Junior (Carden 1991) and in the Green Springs Mine (Wilson and others 1991).

The Pennsylvanian Ely Limestone is found on the western flank of the Cherry Creek Range approximately 15 km south of the Golden Butte Mine. The contact between this very thick (651 m) unit and the Chainman Shale has been interpreted by Fritz (1968) to be a thrust. However, to the east in the Egan Range, Ely Limestone lies conformably upon the Chainman Shale.

Tertiary rhyolitic welded ash-flow tuffs and andesitic to silicic lavas are exposed to the north and west of the Golden Butte Mine. Although none of these units have radiometric ages, they are assumed to be middle Tertiary (35–30 Ma) in age based on regional relationships (e.g., Gans and others 1989). Four volcanic units were mapped by Hasler (1985). The lowest is a flow-layered, phenocryst-rich (25%) intermediate composition lava flow. Phenocrysts consist of hornblende, biotite, and plagioclase. A welded ash-flow tuff of the same mineralogy is present locally. A rhyolitic welded tuff containing 25% sanidine, plagioclase, smoky quartz, and biotite phenocrysts overlies the preceding unit. A third phenocryst-poor welded ash-flow tuff is exposed in isolated areas, but its stratigraphic relation to the other units is impossible to determine. Near the mine, the volcanic rocks are faulted against Devonian and Mississippian units. Similar volcanic units to the north lie unconformably upon the Permian Arcturus Formation (Hose and Blake 1976), indicating substantial offset on one or more sets of faults, the existence of prevolcanic topography, or most likely folding and erosion before middle Tertiary volcanism.

Quaternary colluvium and alluvium surrounding Golden Butte consist of unconsolidated boulders of jasperoid and dolomite, sand, silt, and caliche. Thickness of this unit is generally less than 15 m, but it reaches more than 100 m, measured by drilling, southwest of the ore deposit in a large graben on the east side of Black Mountain (fig. 1).

### *Structure*

Geologic mapping and drilling has revealed both low- and high-angle faults within the Golden Butte pit and the adjacent area. A low-angle fault, interpreted by mine geologists as a thrust fault (Hasler 1985), superposes the Simonson Dolomite on the Chainman Shale (fig. 2). The fault is exposed in the uppermost levels of the mine and extends north and south along the western side of the range. Drilling in the pit has also revealed what appears to be the Simonson Dolomite beneath the Chainman Shale (fig. 3). An initial stage of thrusting of the Chainman Shale over the Simonson Dolomite and subsequent thrusting of Simonson Dolomite over the Chainman Shale could explain the apparent superposition of units. The thrusting of a usually incompetent unit like the Chainman Shale seems unlikely; moreover, thrusting of a younger unit over an older unit is unlikely unless the rocks were folded or otherwise deformed prior to thrusting. In this region, contractional tectonics are thought to be Mesozoic in age. An alternative, and perhaps simpler, interpretation of the subhorizontal faults is that they are low-angle normal faults of the sort mapped by Gans (1982) and Gans and others (1989) in the adjacent Egan Range. These low-angle faults developed during the Tertiary.

The low-angle faults are cut by high-angle faults probably related to late Tertiary basin-and-range extension. In the mine area, these faults have two distinctive strikes, northwest and northeast. Two prominent northeast-striking normal faults are located just west of the mine on the west side of Black Mountain (fig. 1). East of Black Mountain a fault sympathetic to the one mentioned above forms a horst and causes a repetition of units found to the east. Another northeast-striking normal fault places middle Tertiary volcanic rocks against the Simonson Dolomite just north of the mine (fig. 1). The maximum amount of vertical displacement along this fault is estimated to be 3 km, assuming the Paleozoic units were neither thickened nor thinned by low-angle faulting and that the beds were horizontal at the time of eruption of the volcanic rocks (N. A. Johnson written communication 1988). If the Golden Butte deposit was formed prior to movement along this fault (that is, before late Tertiary), 3 km could represent the maximum depth of formation of this deposit. Seedorff (1991), assuming the deposit formed in the Tertiary, estimated the

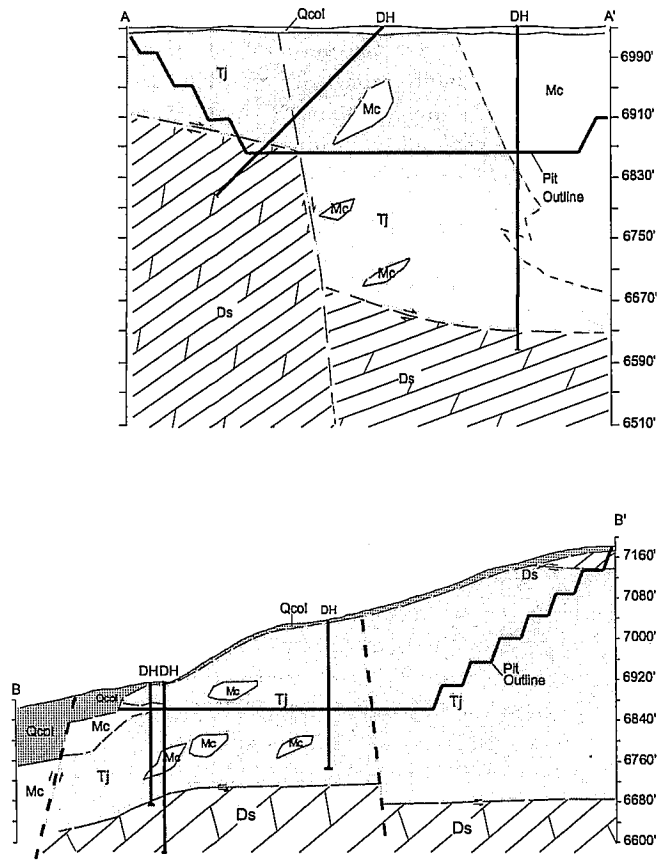


FIGURE 3.—*Cross sections through the pit at Golden Butte drawn using information obtained from drill logs and surface geology. Locations for A-A′ and B-B′ are shown in figure 2. The topographic profiles represent the surface prior to mining. Outlines of the pit (solid lines) at the time of excavation of the 6868-foot elevation level are also shown. Lenses of Chainman Shale within the Tertiary jasperoid are a diagrammatic representation of the discontinuous nature of the jasperoid. Positions of faults and changes in lithology, other than in areas that intersected drill holes (DH), are inferred.*

depth of formation of the Golden Butte deposit to be 1 to 2 km based on a structural reconstruction of the northern Egan and southern Cherry Creek Ranges.

Two high-angle faults are exposed in the Golden Butte pit (fig. 2). The most obvious is almost vertical and strikes between N 45° W and N 65° W (figs. 2 and 3) and has brought the Simonson Dolomite in contact with the Chainman Shale. The amount of displacement on this fault is unknown due to the repetition of the Simonson Dolomite by low-angle faulting. Drill logs, obtained before mining, suggest the downthrown side of the northwest-striking fault lies to the northeast (fig. 3). Following this interpretation, the Simonson Dolomite exposed in the southwest portion of the mine represents the dolomite unit beneath the lower low-angle fault. Another fault striking N 55° E displaces the northwest-striking fault about 20 m. Apparent vertical displacement, as seen from beds in the pit wall, is not much more than 15 m with the downthrown side to the south. Normal or right-lateral strike-slip movement could produce the observed displacement along this fault.

### *Jasperoid*

A large body of hard, massive, "hammer-ringing" jasperoid is located in the Chainman Shale, beneath the low-angle fault in the eastern wall of the mine. This jasperoid increases in apparent width from approximately 25 m at the 6,865-foot level to 50 m near the low-angle fault contact with the Simonson Dolomite (fig. 4). Drillhole data shows that this jasperoid is part of a larger body that extends into the pit and is the major host of gold ore. The dolomite in the upper plate evidently acted as an impermeable or unreactive barrier for hypogene hydrothermal fluids that created the jasperoid. These silica-bearing fluids appear to have collected beneath the dolomite, silicifying and mineralizing the Chainman Shale below the fault contact. Other jasperoid bodies, forming the North Golden Butte deposit and nearby barren outcrops, are found along the trace of this low-angle fault where it is exposed north of the mine.

Brecciation is evident throughout the mine within both the Chainman Shale and jasperoid. In the jasperoid, breccias are weakly to well cemented and show evidence for multiple episodes of silicification. Fragmentation may have occurred by solution and collapse as well as by faulting. Loosely consolidated breccias located between the jasperoid body beneath the low-angle fault and the northwest-striking fault are most likely related to repeated movement along the fault. These breccias contain angular to subrounded jasperoid clasts within the highly contorted and argillically altered Chainman Shale. Breccia consisting of angular shale or siltstone clasts supported by a clay matrix is also present in some areas within the Chainman Shale and may represent argillic alteration of a tectonic or solution breccia.

### *Gold Distribution*

The ore at Golden Butte lies in a lobate, semicontinuous body hosted in jasperoid beneath the low-angle fault. Cutoff grade for the ore is 0.008 oz/ton gold (0.27 ppm), and only a small percentage of ore contains more than 0.05 oz/ton gold (1.7 ppm) (fig. 5). The highest gold concentrations are near the northeast-trending normal fault and decrease in an irregular fashion away from it. Ore grades tend to drop abruptly at the ore/waste boundaries. These boundaries are generally coincident with the traces

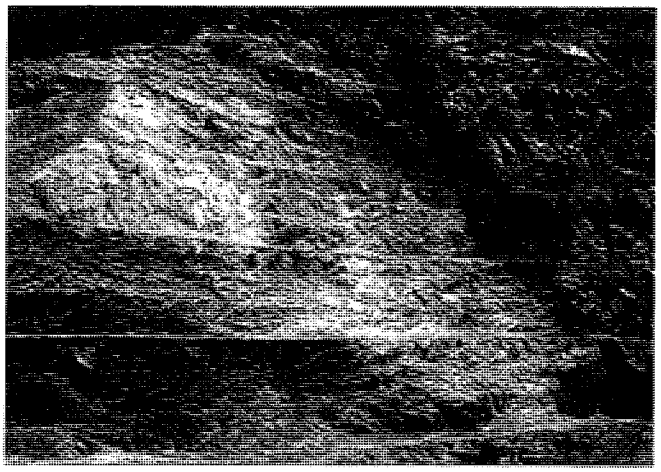

FIGURE 4.—*Photograph of eastern wall of the Golden Butte pit. Jasperoid body (dark gray on right) enlarges substantially near the contact with the low-angle fault (off photo to top). A carbonaceous zone (black) in the Chainman Shale (light gray) is present to the left of the jasperoid and to the right of argillically altered Chainman Shale (light). The contact between the jasperoid and the Chainman Shale is a high-angle normal fault. Benches are approximately 10 meters high.*

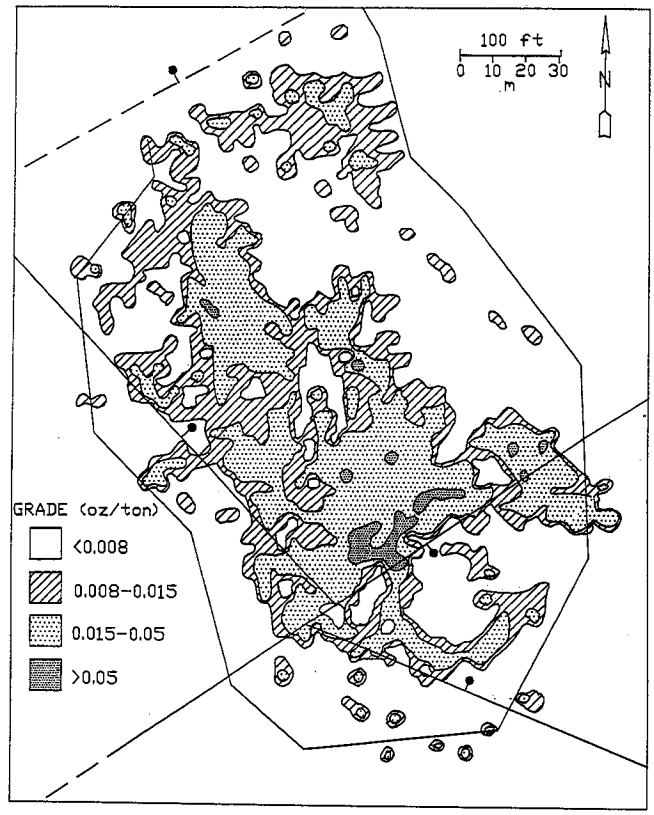


FIGURE 5.—*Grade contour map for Au on the 6,865-foot elevation level with pit outline and normal faults. The information used to construct this map was gathered from analyses of cuttings taken from blast holes drilled on a 50-foot grid in the pit. The close association of ore grade gold and faults suggests that these faults acted as conduits for flow of gold-bearing hydrothermal fluids.*

of the major normal faults. Most of the mineralization lies within the jasperoid body in the Chainman Shale, but mineralization occurs in the Simonson Dolomite along its fault contacts with the Chainman Shale. Thus, the shape of the ore body appears to be controlled by the location of the northeast- and northwest-striking high-angle faults and the distribution of the Chainman Shale host. Because gold mineralization and jasperoid correspond closely to the positions of the high-angle faults, we conclude that these faults formed before mineralization and that they served as important pathways for the mineralizing fluids that formed the jasperoid and deposited gold beneath the low-angle fault (fig. 5).

Of the 72 samples collected in the pit, 39 had gold concentrations greater than the detection limit of 0.05 ppm. Of these, 27 are jasperoids (table 3). Many of the other samples with significant gold concentrations were collected along or near the two high-angle faults (examples GB-22, GB-23, GB-24, GB-26, GB-49, CP2-1; fig. 6) in argillized Chainman Shale and in the Simonson Dolomite (table 3).

## HYDROTHERMAL ALTERATION

The major types of hydrothermal alteration associated with sediment-hosted, disseminated gold deposits (carbonate removal, silicification, argillization, carbonatization, dolomitization, and oxidation) are all present at the Golden Butte deposit. The type and extent of alteration and mineralization at Golden Butte were controlled by permeability and reactivity of the host rocks as well as by the position of the faults.

In the Chainman Shale (fig. 4), the most evident products of alteration are jasperoid, argillically altered rocks, and carbonaceous zones. Jasperoid also contains coarsely crystalline quartz, and stibnite ($Sb_2S_3$), and, where oxidized, stibiconite ($Sb_3O_6(OH)$) and barite ($BaSO_4$). The enclosing argillically altered Chainman Shale is a buff claystone or siltstone that is typically decalcified, strongly bleached and oxidized, and lacks persistent bedding. Irregular carbonaceous zones are present within the Chainman Shale throughout the mine, commonly along the margins of jasperoid.

Within the Simonson Dolomite, hydrothermal alteration is not as obvious as in the Chainman Shale and gold mineralization is extremely limited. Radtke and others (1980) and Bakken and Einaudi (1986) found hydrothermal dolomite at Carlin, and Hofstra and others (1991)

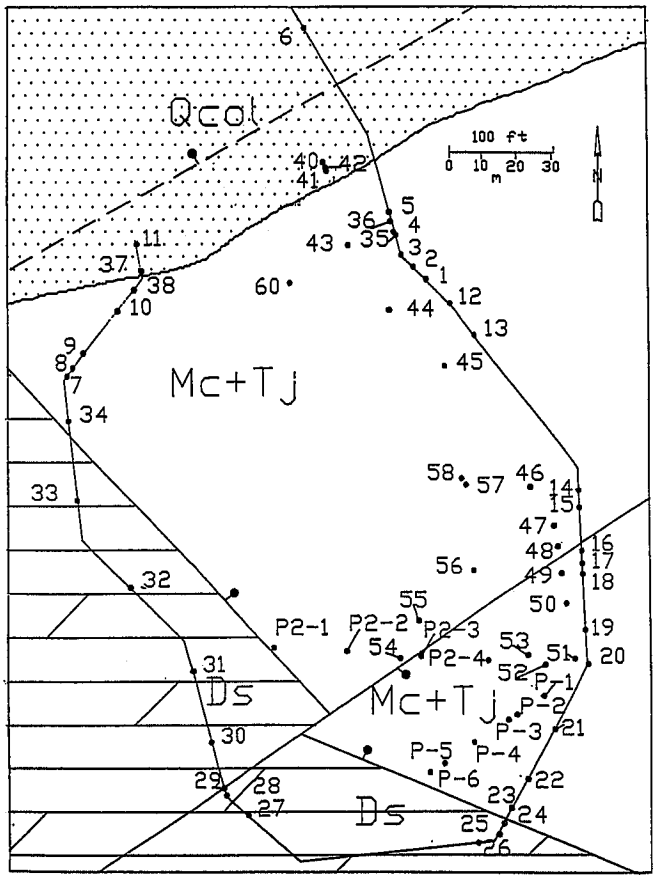


FIGURE 6.—*Location of samples collected on 6,865-foot and 6,850-foot elevation levels with pit outline and geology. All sample numbers have a GB or C prefix. Symbols are the same as in figure 2, but jasperoid and Chainman Shale are not differentiated.*

have shown that dolomite may be a common product of hydrothermal alteration in sediment-hosted gold deposits. Thus, secondary dolomite that equilibrated with the ore-forming fluid might be difficult to distinguish from unaltered rock in the Simonson Dolomite at Golden Butte. Calcite veins, jasperoid breccia cemented by calcite, and minor quartz veins are associated with small bodies of jasperoid in the Simonson Dolomite. Stibiconite and stibnite occur within some of these jasperoids. Beds altered to clay and irregular masses of sanded dolomite are the only other obvious alteration products found in the Simonson Dolomite. Mineralization and obvious alteration are restricted to argillically altered bedded units and to areas next to high-angle faults, suggesting that these faults preceded mineralization.

## JASPEROIDS

The most prominent product of silicification in the mine area is jasperoid. In the Chainman Shale, the contact of the jasperoid bodies with the argillically altered host is sharp and well defined. Jasperoid in the Simonson Dolomite is not everywhere as clearly defined. In the uppermost levels of the mine and in the western wall of the pit, weakly silicified dolomite and jasperoid are interbedded with argillically altered rocks.

The megascopic features of the jasperoid in the Golden Butte Mine vary greatly, even in samples that were collected within a meter of each other. The color of weathered surfaces is most commonly red to dark reddish brown. Fresh surfaces of the denser, less vuggy jasperoid are generally dark gray to medium brown gray. This type of brecciated jasperoid commonly contains lighter-colored fragments of older jasperoid or silicified Chainman Shale in a dark gray matrix (fig. 7a). Highly brecciated, vuggy outcrops tend to be heavily stained with iron oxides. Fractures are prevalent in every exposure of jasperoid within the mine. The fractures are stained red due to oxidation of original pyrite in the jasperoid and/or deposition of secondary iron oxides—limonite or hematite. From these field relationships we infer that the oxidation was caused by descending, oxidized meteoric waters rather than late hydrothermal fluids.

Breccias within the jasperoid developed from disruption of sedimentary units followed by silicification as well as by brecciation of jasperoid followed by deposition of a second generation of jasperoid within voids. Tectonic and solution collapse brecciation appear to have been important. However, field examination and XRF analysis show that easily soluble carbonate is not the dominant constituent of unaltered Chainman Shale. A representative sample of unaltered Chainman Shale (GB-63) has 17.7 wt percent CaO and MgO (table 1), apparently in carbonate minerals. Removal of all of this carbonate could not produce the amount of brecciation found in the pit. Moreover, breccias of preexisting jasperoid are common. These observations preclude solution as the sole cause of brecciation in the deposit. Evidence of fault-related brecciation is present on the east side of the pit in the jasperoid adjacent to the northwest-trending fault. This breccia was the result of shattering of preexisting jasperoid followed by weak silicification of the fragments and oxidation of iron to create a very vuggy and iron-stained rock (fig. 7b). It is worth reemphasizing here that jasperoid is best developed along low-angle faults in this part of the Cherry Creek Range. These faults may have also created brecciation and attendant open spaces that were later filled.

Vugs, created by the replacement process or by brecciation, are highly variable in size and show random orientations and distributions within the jasperoid bodies. Vugs having no apparent association with brecciation tend to be small (< 1 cm), rounded, and uncommon. Vugs between breccia clasts are large (several cm), angular, and

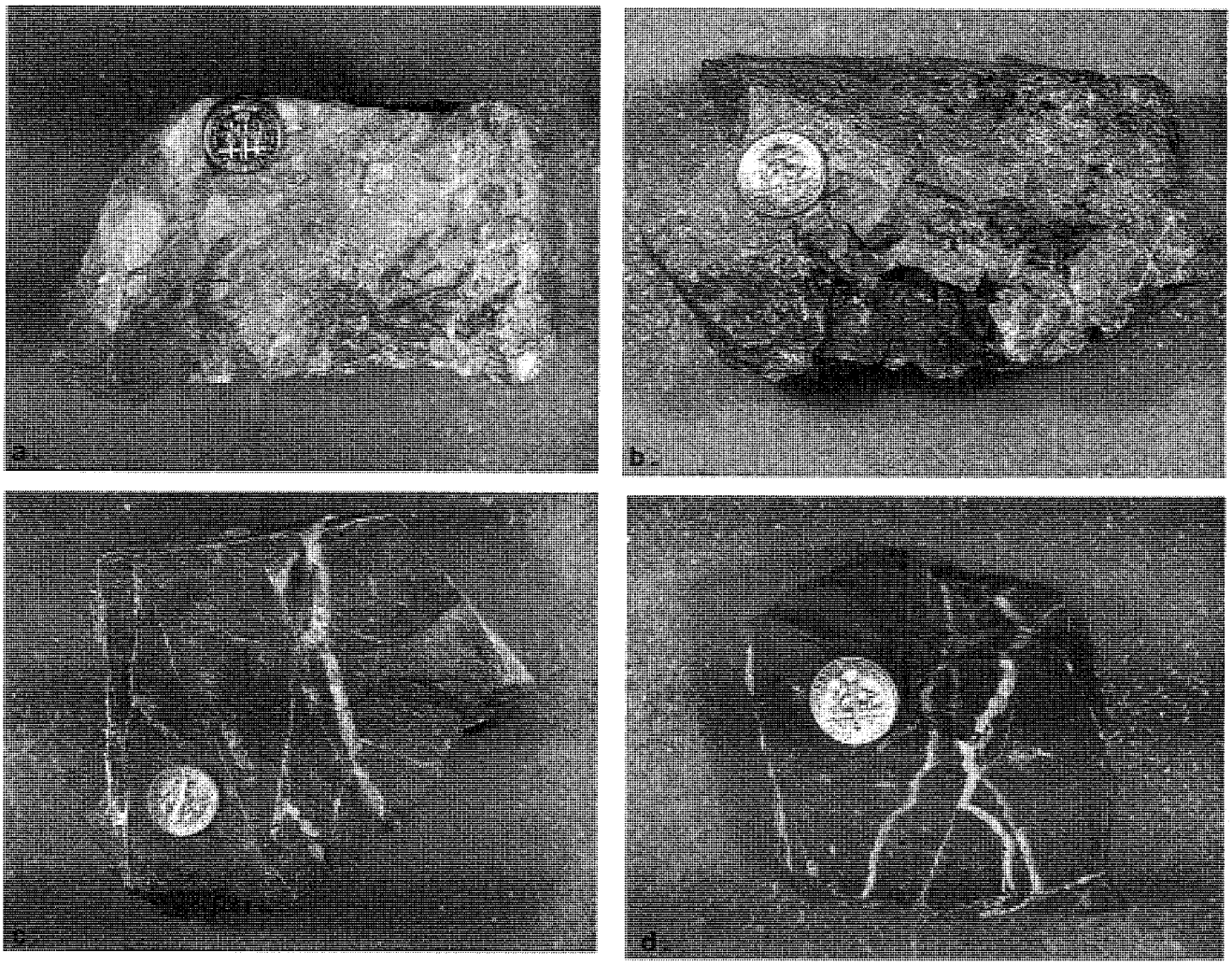

FIGURE 7.—*Jasperoids from the Golden Butte Mine: (a) Brecciated jasperoid containing light-colored jasperoid fragments in a darker jasperoid matrix with some small vugs (sample GB-4), (b) vuggy and iron-stained brecciated jasperoid (GB-48), (c) quartz veins crosscutting dense jasperoid, (d) chalcedony and quartz veins cutting dark, dense jasperoid (GB-36).*

common. Both types of vugs are characteristically lined with coarser quartz, locally accompanied by stibnite. In oxidized vuggy rocks, hematite, barite, and stibiconite replacements of stibnite are present with quartz.

Relict textures of the host rock are uncommon in jasperoids at Golden Butte; relict bedding is preserved locally in jasperoid within the Simonson Dolomite. Relict bedding in jasperoid within the Chainman Shale was found only in one location. No other sedimentary structures, fossils, or carbonate pseudomorphs were identified.

Grain size in jasperoid as seen in thin sections is highly variable. Commonly, these differences are related to different periods of deposition of quartz in the jasperoid. Examples of this heterogeneity include fine-grained groundmass cut by coarser quartz veins (fig. 8a), quartz-lined or filled vugs in a matrix of fine-grained quartz (fig. 8b), and fine-grained breccia fragments in a coarse-grained matrix. Individual quartz grains range in diameter from less than 0.01 mm to over 1 cm. The finer-grained quartz (around 0.01 mm) is by far the most common. Where more than one generation of quartz is present, such as in vugs, veins, and breccias, the later generation is generally coarser grained and shows a wider range of grain sizes than the earlier jasperoid. Jigsaw-puzzle texture (Lovering 1972) is characteristic of the fine-grained jasperoid and consists of highly irregular, uniform-sized quartz grains that tightly interlock. Coarser-grained quartz exhibits a more granular texture in which the grains are nearly equant and have simple boundaries.

The jasperoid bodies preserve evidence of multiple silicification and brecciation events produced during numerous episodes of veining at Golden Butte. Veins

*Table 1.—Composition of Whole Rocks from Golden Butte as Analyzed by XRF (wt%).*

| Sample No. | $SiO_2$ | $TiO_2$ | $Al_2O_3$ | $Fe_2O_3$ | MnO | MgO | CaO | $Na_2O$ | $K_2O$ | $P_2O_5$ | Total | S | LOI | General* Lithology |
|---|---|---|---|---|---|---|---|---|---|---|---|---|---|---|
| GB-2 | 33.8 | 0.26 | 6.80 | 3.47 | 0.05 | 20.99 | 32.41 | 0.00 | 1.25 | 0.14 | 99.2 | 0.04 | 33.3 | Arg Mc |
| GB-5 | 67.7 | 1.20 | 23.01 | 5.11 | 0.01 | 0.78 | 0.26 | 0.13 | 2.74 | 0.22 | 101.2 | 0.97 | 9.7 | Carb Mc |
| GB-9 | 62.7 | 0.46 | 9.05 | 21.22 | 0.01 | 1.31 | 0.31 | 0.03 | 2.87 | 0.23 | 98.2 | 1.13 | 5.9 | Arg Mc |
| GB-24 | 39.5 | 0.05 | 51.68 | 1.02 | 2.50 | 1.39 | 1.42 | 0.09 | 0.27 | 0.21 | 98.2 | 0.36 | 23.7 | Arg Mc |
| GB-32 | 62.5 | 0.94 | 18.61 | 7.94 | 0.01 | 2.15 | 1.03 | 0.12 | 5.73 | 0.22 | 99.2 | | 5.5 | Arg Mc |
| GB-53 | 29.7 | 0.00 | 59.33 | 0.17 | 0.00 | 0.12 | 0.11 | 1.30 | 7.08 | 0.15 | 97.9 | 9.63 | 36.9 | Arg Mc |
| GB-63 | 60.5 | 0.61 | 12.02 | 5.63 | 0.05 | 7.27 | 10.44 | 0.03 | 2.98 | 0.15 | 99.7 | 1.80 | 18.7 | Arg Mc |
| GB-23 | 14.1 | 0.00 | 4.41 | 0.85 | 0.29 | 31.40 | 45.72 | 0.02 | 0.06 | 0.10 | 96.9 | | 42.7 | dolomite |
| GB-25 | 5.2 | 0.02 | 0.12 | 0.14 | 0.02 | 38.42 | 55.00 | 0.00 | 0.07 | 0.04 | 99.0 | 0.04 | 45.4 | dolomite |
| GB-62 | 5.3 | 0.01 | 0.00 | 0.00 | 0.01 | 38.98 | 54.79 | 0.00 | 0.04 | 0.05 | 99.2 | 0.05 | 45.2 | dolomite |
| GB-3 | 89.3 | 0.18 | 4.21 | 1.48 | 0.01 | 0.90 | 1.15 | 0.01 | 1.02 | 0.06 | 98.3 | 0.06 | 2.9 | jasperoid |
| GB-10 | 97.9 | 0.04 | 1.49 | 1.11 | 0.01 | 0.19 | 0.26 | 0.01 | 0.14 | 0.03 | 101.2 | 0.00 | 1.3 | jasperoid |
| GB-13 | 93.6 | 0.02 | 4.17 | 0.41 | 0.01 | 0.00 | 0.08 | 0.04 | 3.26 | 0.03 | 101.6 | 0.04 | 0.5 | jasperoid |
| GB-17 | 99.1 | 0.06 | 1.27 | 1.68 | 0.01 | 0.13 | 0.10 | 0.01 | 0.13 | 0.06 | 102.6 | 0.02 | 0.5 | jasperoid |
| GB-18 | 97.8 | 0.04 | 1.75 | 2.36 | 0.01 | 0.02 | 0.06 | 0.05 | 0.20 | 0.08 | 102.3 | 0.22 | 1.6 | jasperoid |
| GB-29 | 84.8 | 0.18 | 4.10 | 1.32 | 0.01 | 0.68 | 2.97 | 0.04 | 1.08 | 0.06 | 95.2 | | 3.5 | jasperoid |
| GB-30 | 67.3 | 0.01 | 1.85 | 0.57 | 0.02 | 1.27 | 17.89 | 0.04 | 0.34 | 0.05 | 89.4 | | 15.5 | jasperoid |
| GB-35 | 58.2 | 0.17 | 2.38 | 1.26 | 0.01 | 0.33 | 0.68 | 0.13 | 0.47 | 0.04 | 63.6 | 2.05 | 3.4 | jasperoid |
| GB-36 | 91.8 | 0.18 | 3.62 | 1.79 | 0.01 | 0.42 | 0.28 | 0.04 | 0.91 | 0.05 | 99.1 | 0.07 | 1.6 | jasperoid |
| GB-51 | 92.9 | 0.32 | 4.86 | 1.87 | 0.01 | 0.06 | 0.06 | 0.07 | 1.01 | 0.18 | 101.3 | 0.21 | 1.9 | jasperoid |
| GB-54 | 92.5 | 0.12 | 3.37 | 2.18 | 0.01 | 0.11 | 0.19 | 0.08 | 0.63 | 0.05 | 99.2 | 0.04 | 2.2 | jasperoid |
| GB-55 | 94.6 | 0.13 | 2.71 | 1.71 | 0.01 | 0.26 | 0.08 | 0.01 | 0.54 | 0.07 | 100.1 | 0.07 | 1.1 | jasperoid |
| CP-6 | 96.6 | 0.11 | 2.40 | 1.27 | 0.00 | 0.13 | 0.06 | 0.02 | 0.58 | 0.03 | 101.2 | 0.13 | 1.1 | jasperoid |
| CP2-2 | 94.7 | 0.15 | 3.21 | 2.95 | 0.02 | 0.13 | 0.11 | 0.03 | 0.70 | 0.05 | 102.0 | 0.00 | 1.3 | jasperoid |

space = not analyzed
*More complete descriptions in table 3
LOI = Loss on Ignition at 1000 C for 4 hours
Abbreviations: Mc = Chainman Shale, Arg = argillically altered, Carb = Carbonaceous

*Table 1 (continued).—Composition of Whole Rocks from Golden Butte as Analyzed by XRF (ppm).*

| Sample No. | Sc | V | Ni | Cu | Zn | Ga | Rb | Sr | Y | Zr | Nb | Ba | La | Ce | Nd | Th | General* Lithology |
|---|---|---|---|---|---|---|---|---|---|---|---|---|---|---|---|---|---|
| GB-2 | | 49 | 75 | 11 | 239 | 7 | 63 | 212 | 10 | 72 | 8 | 47 | 12 | 39 | 11 | 3 | Arg Mc |
| GB-5 | 26 | 197 | 74 | 22 | 111 | 27 | 170 | 417 | 28 | 218 | 22 | 120 | 41 | 92 | 32 | 19 | Carb Mc |
| GB-9 | 110 | 380 | 9 | 27 | 10 | 31 | 118 | 142 | 71 | 119 | 12 | 266 | 11 | 75 | 14 | 156 | Arg Mc |
| GB-24 | 14 | 17 | 2089 | 117 | 2968 | 3 | 5 | 59 | 232 | 18 | | 600 | | 12 | 4 | | Arg Mc |
| GB-32 | 21 | 147 | 102 | 30 | 153 | 25 | 235 | 57 | 35 | 181 | 21 | 206 | 41 | 385 | 25 | 31 | Arg Mc |
| GB-53 | 13 | 3 | 23 | 47 | 132 | 1 | 91 | 175 | | 2 | 2 | 44 | | | | | Arg Mc |
| GB-63 | 11 | 105 | 90 | 26 | 123 | 15 | 133 | 136 | 23 | 147 | 12 | 169 | 21 | 39 | 22 | 7 | Arg Mc |
| GB-23 | | 30 | 357 | 2 | 847 | | 6 | 63 | 46 | 22 | 2 | 60 | 15 | 140 | 20 | | dolomite |
| GB-25 | | 3 | 15 | | 62 | 3 | 7 | 66 | 1 | 30 | 3 | 14 | | | 7 | | dolomite |
| GB-62 | | 3 | 5 | | 6 | 2 | 2 | 72 | | 24 | 2 | 38 | 22 | 3 | | | dolomite |
| GB-3 | 4 | 32 | 15 | 14 | 30 | 5 | 47 | 219 | 4 | 38 | 4 | 64 | 10 | 19 | 10 | 2 | jasperoid |
| GB-10 | 1 | 1 | 10 | 9 | 4 | 2 | 12 | 11 | 1 | 20 | 1 | 42 | | | | | jasperoid |
| GB-13 | 2 | 3 | 15 | 26 | 9 | 6 | 196 | 89 | 2 | 10 | 1 | 28 | | | | | jasperoid |
| GB-17 | 2 | 9 | 15 | 10 | 12 | | 9 | 114 | 3 | 15 | 3 | 70 | | 1 | 6 | 3 | jasperoid |
| GB-18 | 9 | 5 | 24 | 9 | 14 | 1 | 11 | 95 | 3 | 16 | 2 | 261 | | 5 | 1 | 5 | jasperoid |
| GB-29 | 5 | 59 | 28 | 25 | 26 | 6 | 70 | 39 | 10 | 69 | 7 | 87 | 27 | 152 | 5 | 7 | jasperoid |
| GB-30 | 98 | 21 | 10 | 5 | 32 | | 19 | 52 | 52 | 16 | 1 | 123 | 1 | 71 | 9 | 197 | jasperoid |
| GB-35 | 177 | 221 | 9 | 6 | 13 | 1 | 5 | 130 | 52 | 18 | | 162531 | | | 42 | 126 | jasperoid |
| GB-36 | 45 | 29 | 16 | 16 | 20 | 5 | 37 | 56 | 22 | 42 | 5 | 3138 | | 17 | 5 | 45 | jasperoid |
| GB-51 | 4 | 47 | 11 | 16 | 15 | 7 | 40 | 487 | 9 | 50 | 7 | 83 | 7 | 31 | 9 | 3 | jasperoid |
| GB-54 | 56 | 18 | 16 | 27 | 187 | 3 | 31 | 48 | 23 | 32 | 3 | 83 | | 14 | 1 | 55 | jasperoid |
| GB-55 | 5 | 17 | 12 | 17 | 19 | 3 | 26 | 29 | 3 | 31 | 3 | 3 | 94 | 5 | 13 | 5 | jasperoid |
| CP-6 | 24 | 15 | 11 | 9 | 7 | 3 | 28 | 10 | 8 | 31 | 2 | 33 | 7 | 14 | 4 | 19 | jasperoid |
| CP2-2 | 8 | 30 | 27 | 22 | 55 | 4 | 45 | 35 | 14 | 40 | 5 | 38 | 6 | 39 | 7 | 6 | jasperoid |

space = below 1 ppm
*More complete descriptions in table 3
Abbreviations: Mc = Chainman Shale, Arg = argillically altered, Carb = Carbonaceous

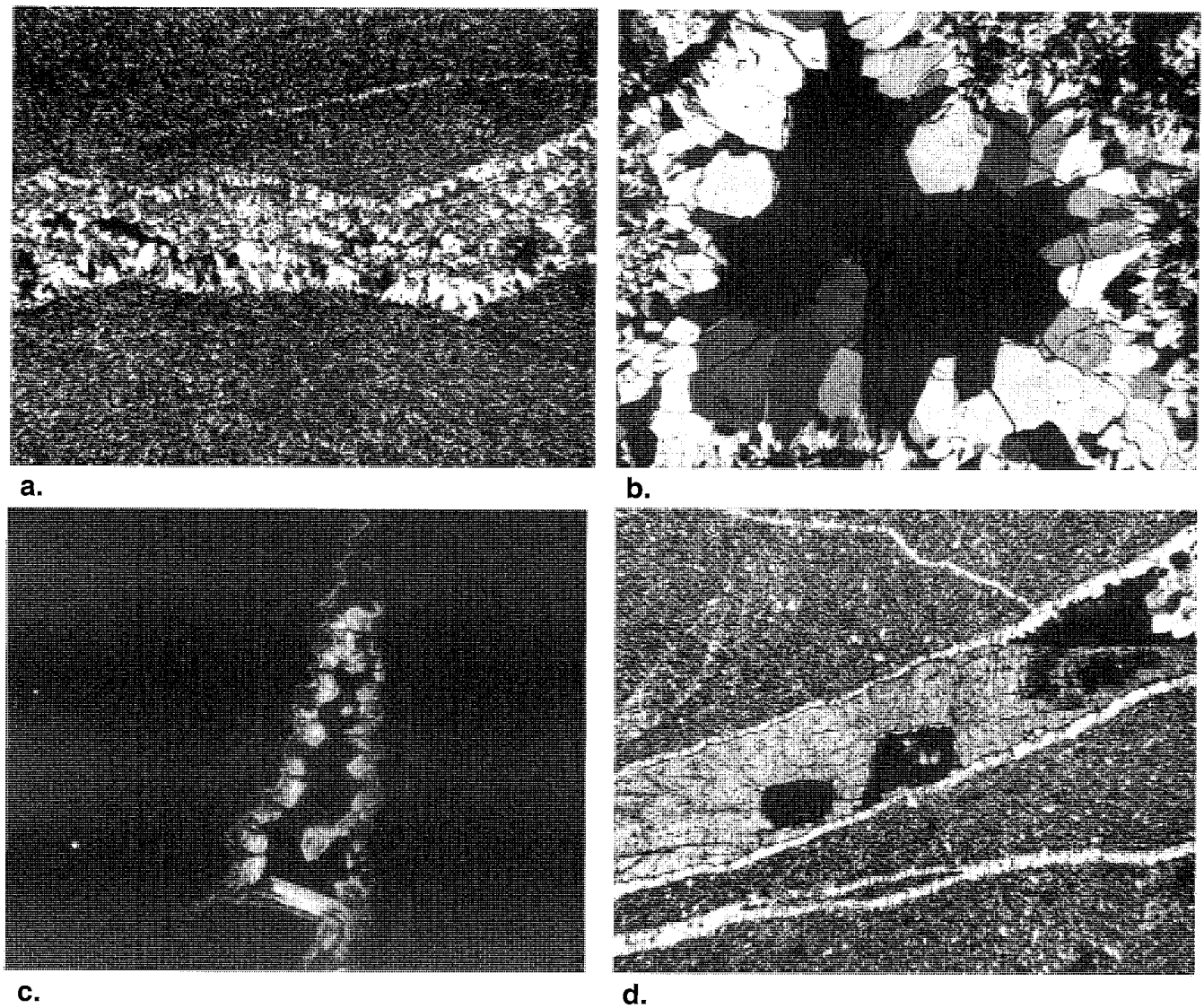


FIGURE 8.—*Photomicrographs of jasperoid samples under cross polarized light. Each photograph is approximately 3 mm x 2 mm. (a) Quartz vein cutting fine-grained jasperoid (GB-36), (b) vug containing quartz grains exhibiting elongation along the c-axis and pyramidal terminations (CP2-2), (c) cathodeluminoscope photograph of zoned quartz in a vug (CP2-2), (d) quartz-lined barite vein cutting fine-grained jasperoid (GB-35).*

crosscut many textural features of the jasperoids (including breccias, vugs, and other veins) and appear to be part of a later stage of mineralization. Within the voluminous jasperoids in the Chainman Shale, the most common vein mineral is quartz (fig. 7c). Calcite is the most common vein-filling mineral in the jasperoids formed within the Simonson Dolomite. Chalcedony (fig. 7d), iron oxides, and barite are less common vein-filling minerals. Pyrite is also present in some quartz veins in jasperoid.

Accessory minerals in jasperoids may represent older minerals that have remained unreplaced during silicification, minerals formed contemporaneously with silicification, or minerals formed after the main silicification (Lovering 1972). Some fine-grained minerals observed in thin sections must represent clay remnants of the original shale host, as indicated by the geochemical analysis (see below). Jasperoid that is not brecciated or veined may have formed during one period of silicification. Thus, accessory minerals in these jasperoids may have formed contemporaneously with silicification. Stibnite is commonly found in unoxidized, nonbrecciated jasperoid. It forms rosettes and isolated prismatic orthorhombic crystals in the jasperoid

groundmass and multiple blades radiating from a point in vugs. Pyrite crystals are small, but fairly common within the jasperoid groundmass. Cinnabar and realgar have also been reported (N. A. Johnson written communication 1990) within unoxidized jasperoid. Late-formed accessory minerals are found in veins and in brecciated jasperoid. Quartz, the most common accessory mineral, is characteristically more coarsely crystalline and shows more variation in size than the jasperoid-forming quartz. Quartz grains within veins are commonly elongated parallel to their c axes, show crystal faces and pyramidal terminations, and growth zoning (fig. 8c). Changes in the concentrations of trace elements in the hydrothermal fluids present during several phases of crystal growth could produce this cathodoluminescent zoning. Calcite forms veins and cements breccia in the jasperoid near or in the Simonson Dolomite. Stibiconite occurs in the strongly oxidized and brecciated jasperoid, commonly coexisting with stibnite, and nearly always as stibnite pseudomorphs. Barite is not common in the pit, but it occurs locally with brecciated jasperoid, in quartz-lined veins (fig. 8d), within vugs, with Fe oxides, and with stibiconite.

*Table 2.—Comparison of Lovering's (1972) and Golden Butte Jasperoids (wt%).*

| | Golden Butte Jasperoid | | Lovering's Jasperoid | |
|---|---|---|---|---|
| | Range | Average | Range | Average |
| $SiO_2$ | 85–99 | 93.8 | 80–97 | 92.8 |
| $TiO_2$ | 0.2–0.3 | 0.13 | 0.03–0.8 | 0.1 |
| $Al_2O_3$ | 1.3–4.9 | 3.1 | 0.3–4 | 1.4 |
| FeO | * | * | 0.15–0.7 | 0.4 |
| $Fe_2O_3$ | 0.41–3.0 | 1.7 | 0–5 | 1.3 |
| MnO | 0–0.02 | 0.01 | ** | ** |
| MgO | 0–0.9 | 0.25 | 0–1 | 0.2 |
| CaO | 0.06–3.0 | 0.45 | 0–1 | 0.4 |
| $Na_2O$ | 0.01–0.0 | 0.03 | 0–0.3 | 0.1 |
| $K_2O$ | 0.13–3.3 | 0.85 | 0.1–1 | 0.3 |
| $P_2O_5$ | 0.03–0.1 | 0.06 | 0.01–0.4 | 0.1 |
| S | 0–0.22 | 0.08 | 0–3 | 1.2 |
| Ba | 0–0.3 | 0.03 | 0–0.4 | 0.1 |

*FeO oxidized to $Fe_2O_3$ before analysis
**Not listed by Lovering

*Elemental Composition*

Fourteen jasperoid samples were analyzed by XRF for major elements and sulfur (table 1). $SiO_2$ concentrations in these jasperoids range between 58 and 99 wt percent; 10 of the 14 analyses have $SiO_2$ concentrations of 92 wt percent or greater. Two of the four remaining samples contain significant proportions of accessory barite, stibiconite, and calcite (GB-30 and GB-35). These two samples were excluded from the ranges and averages in table 2. $Al_2O_3$ (1.3 to 4.9 wt %, mean 3.1 wt %) and $Fe_2O_3$ (0.41 to 3.0 wt %, mean 1.7 wt %) are the next most abundant oxides. The ranges and means of major element concentrations of 10 "representative" jasperoid samples collected by Lovering (1972) from the United States (table 2) are similar to the mean composition of the 12 Golden Butte jasperoid samples. In both cases, $SiO_2$, $Al_2O_3$, and $Fe_2O_3$ make up greater than 95 wt percent of the jasperoid, with the other constituents having only minor concentrations. The range and mean of $Al_2O_3$ in the Golden Butte jasperoids are higher than reported by Lovering (1972), probably because the Chainman Shale is an Al-rich protolith, whereas most of Lovering's samples were of jasperoid that replaced carbonate. The only other significant difference lies in the lower average S (0.08 vs. 1.2 wt %) in Golden Butte jasperoid.

Trace-element concentrations in jasperoid samples were determined by ICP (34 samples) and by XRF (14 of 34 samples). Tables 1 and 3 list the results, except Te, which was always below detection of 0.5 ppm. Concentrations of Bi, Se, and Cd in more than half the samples were below detection and are not discussed further. As expected, concentrations of As, Ag, Sb, and Au in average jasperoid are enriched more than 100 times as compared to bulk continental crust as calculated by Taylor and McClennan (1985) (table 4). Thallium, Mo, and Th also show marked increases in concentration over that of typical crustal rocks. On the other hand, Ba, Sr, Zr, Nb, V, Ni, Cu, and Zn in jasperoids are 3 to 11 times less than bulk continental crust.

Trace-element analyses of jasperoids at Carlin, Mercur, Vantage, Drum, and Elephant Head gold deposits, along with samples collected from various mineralized and unmineralized jasperoids from the northern Great Basin (Holland and others 1988, Ilchik 1990, Jewell and Parry 1988, Nutt and others 1991, Radtke and others 1980, Theodore and Jones 1992) display many similarities to the Golden Butte jasperoid (table 5). In most of these jasperoids, the concentrations of the pathfinder elements (As, Ag, Sb, Ba, and Au) are of the same order of magnitude. However, the jasperoids from the Drum Mine and Elephant Head are distinctively enriched in Pb, Zn, and Cu, suggesting that they are related to polymetallic (porphyry-type) mineralization (Nutt and others 1991, Theodore and Jones 1992). The average concentration of Th in the Golden Butte jasperoid is almost 14 times higher (27 vs. 2 ppm) than the geometric mean of 29 jasperoid samples collected by Holland and others (1988) from mineralized jasperoid (including samples from Carlin and Alligator Ridge–Vantage gold deposits) and unmineralized jasperoid.

## ARGILLIC ALTERATION AND CARBONACEOUS ZONES

Argillic alteration at Golden Butte is present in both the Chainman Shale and Simonson Dolomite and appears, from field relations, to have been contemporaneous with the formation of jasperoid. At Golden Butte, argillically altered claystone and siltstone are characterized by their bleached colors and abundance of kaolinite. In the Chainman Shale, the argillic rocks are massive, lacking internal structures. Kaolinite apparently replaced illite, the most common clay mineral in the unaltered shale. These characteristics are consistent with formation of argillic rocks by low-temperature hydrothermal alteration of preexisting phyllosilicate minerals. This alteration is similar to advanced argillic alteration characteristic of aluminosilicates converted to kaolinite, alunite, dickite, pyrophyllite, diaspore, and other aluminum-rich phases (Meyer and Hemley 1967). In many other hydrothermal ore deposits advanced argillic alteration is also associated with silicification.

Argillic alteration in the Simonson Dolomite is found in bedded units in the upper levels of the pit and next to faults. It contains relict bedding and small cavities of coarse-grained calcite. The production of argillic rocks from pure dolomite is difficult to explain because of the lack of preexisting aluminosilicates and the low solubility of Al in hydrothermal fluids. Considering the limited distribution and bedded character of the argillic rocks in the Simonson Dolomite, they probably formed from replacement of silty, clay-rich beds interlayered with beds of clean carbonate. Argillic alteration of silty carbonate rocks is common in other disseminated gold deposits such as Carlin (Radtke 1985) and Mercur (Jewell and Parry 1988).

Typically, the argillic rocks lack organic carbon and contain fine-grained iron oxides that produce their characteristic brown to buff colors. Locally, the argillically altered Chainman Shale (GB-53; fig. 6) contains intimate mixtures of jarosite and kaolinite in white masses. The destruction of organic carbon and sulfides and formation of sulfates occurred during a stage (or stages) of oxidation after the period of mineralization responsible for formation of the jasperoid, initial argillization, and deposition of gold and sulfides. Complete destruction of organic matter and sulfides in a black shale along with the formation of alunite and barite in veins has also been described at the Vantage gold deposit by Ilchik (1990). As at Golden Butte, the period of oxidation at the Vantage deposit follows argillization and gold deposition. However, it is unclear at Golden Butte whether the alteration is a late oxidation event associated with hydrothermal alteration or a product of weathering. We prefer the latter based on the arguments of Seedorff (1991).

Organic carbon was not destroyed in isolated areas of the argillically altered Chainman Shale and around jasperoid bodies contained within it. Although it is unclear how much carbon, if any, was actually introduced during alteration, we simply call these carbonaceous rocks (samples GB-5 and GB-16). It is clear that these samples are not simply unoxidized or unweathered carbonaceous shale from their high concentrations of Sb and As and low Mo (table 3) compared to unmineralized Chainman Shale (GB-63); some alteration before carbon removal occurred. The largest carbonaceous zone lies in the eastern wall of the pit adjacent to the largest jasperoid mass and along the northeast-striking fault (fig. 4). The jasperoid may have acted as an impermeable barrier that prevented the introduction of late oxidizing fluids. Also, the carbonaceous rocks examined are extremely clay rich; destruction of the organic carbon may not have been accomplished due to the lack of permeability in areas containing clay-rich, argillically altered rocks.

### *Elemental Composition*

Seven argillic rocks, including the unaltered Chainman Shale, were analyzed for their major- and trace-element composition. Few complete analyses of argillic rocks from other disseminated gold deposits are available for comparison. As expected, the average composition of the argillic samples (table 4) is more comparable to bulk continental crust than they are to jasperoid. Nonetheless, the pathfinder elements (excluding gold that is below the detection limit) and Th are enriched, as they are in the jasperoid.

Two samples of oxidized, argillically altered Chainman Shale (GB-2 and GB-9) have quite different major-element compositions. Sample GB-53 is very rich in $Al_2O_3$, $K_2O$, and S and poor in $SiO_2$ because it is a mixture of alunite and kaolinite produced by supergene processes. GB-24 is similar in hand sample to GB-53, but low S and $K_2O$ concentrations show that it contains little alunite. This sample was collected along the fault contact between the Simonson Dolomite and the Chainman Shale (fig. 6). Fluids traveling along this fault could have removed silica and other components from the shale protolith, leaving behind aluminum-rich minerals such as gibbsite. The carbonaceous sample (GB-5) is richer in aluminum than the unaltered Chainman Shale (GB-63)—consistent with its clay-rich nature. Argillically altered units of the Simonson Dolomite (GB-32) are similar in major element composition to unaltered Chainman Shale, consistent with the earlier suggestion that its protolith consisted of beds of silty or shaly material in the Simonson Dolomite.

## DOLOMITE-STABLE ALTERATION

Examples of dolomitic alteration are apparent locally at Golden Butte, but dolomite was apparently stable in parts

*Table 3.—Trace Element Concentrations in Whole Rocks from Golden Butte as Analyzed by ICP (ppm)*.*

| Sample | Cu | Zn | Ga | As | Se | Mo | Ag | Cd | Sb | Au | Hg | Tl | Pb | Bi | Sample Description |
|---|---|---|---|---|---|---|---|---|---|---|---|---|---|---|---|
| GB-1 | 2 | 25 | — | 38 | — | 1.6 | 0.034 | 0.50 | 11 | — | 0.4 | 8 | 2 | — | argillically altered Mc |
| GB-2 | 13 | 152 | — | 245 | — | 2.3 | 0.062 | 0.74 | 112 | — | 4.4 | 12 | 7 | — | brecciated argillically altered Mc |
| GB-3 | 9 | 26 | 1 | 87 | — | 4.1 | 0.051 | — | 316 | — | 10.1 | 2 | 25 | — | dense jasperoid |
| GB-4 | 12 | 5 | 3 | 276 | — | 12.2 | 0.333 | — | 443 | 0.463 | 12.8 | 1 | 6 | 0.30 | brecciated jasperoid |
| GB-5 | 17 | 106 | — | 98 | 2.4 | 1.3 | 0.263 | 0.50 | 7 | — | 0.7 | 12 | 9 | — | carbonaceous Mc |
| GB-6 | 1 | 4 | — | 9 | — | 0.5 | 0.036 | — | 754 | — | 0.6 | 1 | 1 | — | jasperoid in Ds |
| GB-7 | *** | *** | *** | 232 | *** | 6.3 | 9.6 | *** | 96000 | 0.425 | 7.3 | 8 | 26 | *** | stibnite + stibiconite in jsp |
| GB-8 | 5 | 3 | 1 | 50 | — | 2.9 | 0.339 | — | — | 0.119 | 2.9 | 2 | 4 | — | dense jasperoid |
| GB-9 | 33 | *** | *** | 1484 | *** | 11.2 | 17.4 | *** | 16700 | 12.3 | 25.6 | 58 | 11 | *** | argillically altered Mc with some jsp |
| GB-10 | 5 | 6 | — | 43 | — | 5.6 | 0.167 | — | 215 | — | 1.4 | 4 | 1 | — | vuggy + veined jasperoid |
| GB-11 | 24 | 2 | 2 | 13 | — | 2.1 | 0.368 | — | 136 | — | 10.3 | 6 | 13 | 0.37 | argillically altered Mc |
| GB-12 | 19 | 49 | 1 | 252 | — | 6.8 | 0.144 | 0.64 | 62 | — | 4.8 | 2 | 16 | 0.37 | brecciated Mc |
| GB-13 | 9 | 3 | — | 4 | — | 3.1 | 58 | — | — | 2.14 | — | 1 | 3 | — | dense jasperoid |
| GB-14 | 20 | 16 | 3 | 160 | — | 18.1 | 0.01 | — | 39 | — | 2.3 | 1 | 10 | 0.70 | argillically altered Mc |
| GB-15 | 14 | 7 | 3 | 1165 | 2.1 | 12.2 | 0.117 | — | 81 | — | 2.1 | 2 | 6 | 0.34 | argillically altered Mc siltstone |
| GB-16 | 30 | 19 | 2 | 537 | 5.6 | 14.3 | 0.355 | — | 123 | — | 1.2 | 4 | 26 | 0.57 | carbonaceous Mc |
| GB-17 | 4 | 12 | — | 293 | 1.1 | 13.2 | 0.094 | — | 393 | — | 3.7 | 3 | 2 | — | Fe stained brecciated jsp |
| GB-18 | 5 | 14 | — | 481 | 2.6 | 13.5 | 2.42 | — | 970 | 3.54 | 39.2 | 34 | 1 | — | quartz veined jasperoid |
| GB-19 | 38 | 60 | 2 | 533 | 1.3 | 5.2 | 0.038 | 0.19 | 1463 | — | 2.6 | 3 | 12 | — | argillically altered Mc |
| GB-20 | 5 | 30 | 1 | 78 | 1.2 | 6.7 | 0.102 | — | 393 | 0.079 | 11.6 | 4 | 14 | — | argillically altered Mc with some jsp |
| GB-21 | 15 | 9 | 4 | 488 | 1.3 | 14.4 | 0.063 | — | 788 | — | 19.0 | 51 | 43 | 0.44 | argillically altered Mc siltstone |
| GB-22 | 22 | 27 | 2 | 488 | 2.0 | 42.0 | 0.129 | — | 2141 | 0.123 | 50.1 | 5 | 39 | 0.81 | argillically altered Mc siltstone |
| GB-23 | 6 | 427 | — | 59 | — | 3.9 | 0.076 | 1.06 | 439 | 0.184 | 1.9 | 50 | 3 | — | sanded Ds |
| GB-24 | 92 | 2650 | — | 218 | — | 23.5 | 0.565 | 2.78 | 625 | 0.724 | 15.9 | 424 | 8 | — | clay material along fault |
| GB-25 | 1 | 22 | — | 8 | — | 1.1 | 0.029 | — | 40 | — | 1.0 | — | 1 | — | apparently unaltered Ds |
| GB-26 | 2 | 111 | — | 25 | — | 2.0 | 0.065 | 0.18 | 174 | 0.119 | 1.2 | 9 | 2 | — | veined calcite in Ds |
| GB-27 | 0.3 | — | — | — | — | 0.2 | 0.243 | — | 18 | — | — | 2 | — | — | massive crystalline calcite |
| GB-28 | 2 | 3 | — | 7 | — | 0.6 | 0.052 | — | 117 | — | 0.6 | 5 | 1 | — | sanded Ds |
| GB-29 | 11 | 12 | 1 | 88 | — | 6.4 | 0.454 | — | 684 | 0.093 | 5.4 | 6 | 6 | — | calcite + quartz veined Ds |
| GB-30 | 3 | 25 | *** | 47 | *** | 2.5 | 2.08 | *** | 21200 | 0.069 | 5.6 | 128 | *** | *** | stibiconite + quartz + calcite in jsp |
| GB-31 | 1 | 7 | — | 5 | — | 0.9 | 0.06 | — | 209 | — | 0.3 | 2 | 1 | — | Bioclastic Ds |
| GB-32 | 32 | 134 | 3 | 338 | 17.9 | 14.2 | 0.092 | — | 2300 | — | 13.7 | 33 | 20 | 0.34 | argillically altered DS |
| GB-33 | 4 | 3 | — | 20 | — | 0.4 | 0.02 | — | 47 | — | 0.3 | 1 | 2 | — | bedded jasperoid in DS |
| GB-34 | 7 | 10 | — | 55 | — | 3.2 | 0.443 | — | 262 | 0.075 | 4.2 | 8 | 4 | — | quartz + calcite veins in jsp |
| GB-35 | 13 | 31 | *** | 137 | *** | 7.3 | 0.409 | *** | 69700 | 0.33 | 4.4 | 14 | 7 | *** | barite + jasperoid |
| GB-36 | 12 | 18 | 1 | 118 | — | 6.0 | 0.843 | 0.16 | 7615 | 0.276 | 4.0 | 15 | 4 | — | quartz + chalcedony veins in jsp |
| GB-37 | 15 | 5 | — | 47 | — | 13.5 | 0.43 | — | 825 | 0.362 | 1.5 | 4 | 3 | — | barite + stibiconite in vuggy jsp |
| GB-38 | 13 | 11 | — | 71 | — | 8.6 | 0.481 | — | 5301 | 0.218 | 11.9 | 84 | 2 | — | vuggy-brecciated jsp |
| GB-39 | 5 | 8 | — | 9 | — | 2.9 | 0.231 | — | 31 | — | 0.9 | 7 | 1 | — | Ds with calcite veins |
| GB-40 | 12 | 12 | 6 | 1291 | 1.2 | 37.2 | 0.324 | — | 359 | 0.062 | 49.8 | 100 | 27 | 0.41 | argillically altered Mc |
| GB-41 | 13 | 16 | *** | 123 | *** | 15.1 | 3.05 | *** | 63800 | 0.504 | 3.8 | 12 | 6 | *** | stibiconite + stibnite in vuggy jsp |
| GB-42 | 22 | 71 | *** | 158 | *** | 7.8 | 3.58 | *** | 83300 | 0.966 | 5.1 | 13 | 7 | *** | barite + stibiconite in vuggy jsp |
| GB-43 | 14 | 143 | *** | 66 | *** | 14.6 | 5.02 | *** | 20100 | 0.248 | 6.1 | 10 | 128 | *** | barite + stibiconite in vuggy jsp |

| | | | | | | | | | | | | | | | |
|---|---|---|---|---|---|---|---|---|---|---|---|---|---|---|---|
| GB-44 | 14 | 7 | 2 | 157 | — | 14.2 | 0.036 | — | 368 | — | 0.3 | 7 | 5 | — | argillically altered Mc siltstone |
| GB-45 | 17 | 8 | 2 | 197 | 1.7 | 9.0 | 0.105 | — | 37 | — | 1.6 | 2 | 22 | — | brecciated argillically altered Mc |
| GB-46 | 11 | 35 | 6 | 764 | — | 29.1 | 0.04 | 0.88 | 51 | — | 0.6 | 2 | 11 | 0.33 | argillically altered Mc |
| GB-47 | 19 | 98 | 47 | 547 | — | 44.6 | 0.068 | 0.57 | 44 | — | 1.1 | 3 | 11 | 0.84 | argillically altered Mc |
| GB-48 | 28 | 96 | 10 | 2510 | 24.2 | 49.6 | 1.73 | 1.32 | 2220 | 0.479 | 185.0 | 36 | 18 | 0.44 | brecciated jasperoid |
| GB-49 | 11 | 38 | 3 | 1731 | — | 33.1 | 0.052 | 0.22 | 802 | 0.047 | 10.6 | 12 | 6 | 0.40 | argillically altered Mc |
| GB-50 | 12 | 34 | 1 | 373 | 1.1 | 9.8 | 0.058 | — | 1869 | 0.094 | 8.6 | 2 | 3 | — | brecciated jasperoid |
| GB-51 | 14 | 16 | 2 | 202 | 1.4 | 13.9 | 0.099 | 0.17 | 125 | — | 1.3 | 2 | 25 | — | jasperoid in bedded Mc |
| GB-53 | 4 | 9 | — | 26 | — | 0.4 | 0.135 | — | 49 | 0.418 | 2.8 | 2 | 1 | — | kaolinite + alunite |
| GB-54 | 23 | 261 | *** | 317 | *** | 9.1 | 6.51 | *** | 8828 | 4.8 | 20.5 | 24 | 16 | *** | vuggy jsp |
| GB-55 | 12 | 20 | — | 268 | — | 19.5 | 2.39 | — | 726 | 2.37 | 3.8 | 18 | 5 | — | dense jasperoid with stibnite |
| GB-56 | 8 | 280 | — | 343 | — | 26.6 | 0.577 | 1.52 | 438 | 0.401 | 32.7 | 52 | 2 | — | quartz veined jasperoid |
| GB-57 | 10 | 11 | — | 618 | 1.8 | 19.0 | 1.09 | — | 412 | 0.968 | 32.5 | 5 | 1 | — | brecciated jasperoid |
| GB-58 | 10 | 5 | 2 | 72 | — | 6.1 | 0.078 | — | 58 | — | 0.4 | 1 | 9 | — | argillically altered Mc |
| GB-59 | 12 | 31 | 1 | 101 | — | 12.0 | 0.447 | — | 804 | 0.128 | 8.1 | 3 | 5 | — | vuggy quartz veined jsp |
| GB-60 | 12 | 20 | 1 | 272 | — | 13.1 | 3.78 | 0.19 | 1747 | 3.54 | 12.4 | 9 | 24 | — | high grade crushed ore |
| GB-61 | 1 | 2 | — | 35 | — | 2.7 | 0.188 | — | 703 | 0.12 | 2.0 | 17 | 1 | — | dense jasperoid |
| GB-62 | 1 | 2 | — | 2 | — | 0.1 | 0.035 | — | 65 | — | 0.2 | 1 | 1 | — | unaltered Ds |
| GB-63 | 26 | 119 | — | 151 | 1.2 | 26.2 | 0.113 | 1.00 | 5 | — | 2.7 | 10 | 13 | 0.57 | unaltered Mc |
| CP-1 | 4 | 19 | 1 | 124 | — | 10.5 | 0.139 | — | 233 | 0.304 | 0.9 | 3 | 6 | 0.35 | argillically altered Mc siltstone |
| CP-2 | 5 | 23 | — | 114 | — | 8.6 | 0.654 | — | 221 | 0.617 | 6.9 | 4 | 5 | — | dense quartz veined jsp |
| CP-3 | 4 | 40 | — | 20 | — | 1.8 | 1.13 | — | 71 | 0.168 | 5.3 | 1 | — | — | kaolinite + alunite |
| CP-4 | 13 | 12 | 6 | 416 | 1.0 | 16.1 | 0.095 | — | 2893 | — | 20.8 | 35 | 22 | 0.29 | argillically altered Mc siltstone |
| CP-5 | 4 | 3 | — | 18 | — | 3.7 | 0.076 | — | 318 | — | 5.1 | 1 | 1 | — | brecciated jasperoid |
| CP-6 | 4 | 6 | 1 | 89 | — | 8.4 | 0.01 | — | 3804 | — | 8.7 | 6 | 5 | — | quartz veined jasperoid |
| CP2-1 | 18 | 103 | — | 181 | — | 13.7 | 2.74 | 0.23 | 7593 | 0.476 | 22.4 | 18 | 6 | — | apparently unaltered Ds |
| CP2-2 | 14 | 56 | — | 494 | — | 37.6 | 0.642 | 0.68 | 573 | 4.87 | 3.6 | 3 | 4 | 0.40 | vuggy quartz veined jsp |
| CP2-3 | 11 | 61 | — | 208 | — | 14.3 | 1.6 | 0.20 | 3612 | 2.69 | 10.7 | 10 | 5 | — | vuggy quartz veined jsp |
| CP2-4 | 4 | 58 | — | 16 | — | 1.9 | 0.032 | 0.68 | 29 | — | 1.2 | 1 | 1 | — | apparently unaltered Ds |
| — | | <1 | <0.5 | <1 | <1 | | | <0.1 | <1 | <0.05 | <0.1 | <0.5 | <0.25 | <0.25 | |
| *** | <0.5 | <10 | <5 | | <10 | | | <1 | | | | | <2.5 | <2.5 | |

Abbreviations: Mc = Chainman Shale, jsp = jasperoid, Ds = Simonson Dolomite
*Concentrations represent fraction not tied up in silicate minerals

*Table 4.—Comparison of Average Golden Butte Jasperoid and Argillic Alteration with Average Upper Continental Crust.*

| | Average Jasperoid (ppm) | Average Argillic* (ppm) | Upper Continental Crust** (ppm) | Fraction Compared to Upper Continental Crust | |
|---|---|---|---|---|---|
| | | | | Jasperoid | Arg.* |
| Sc | 14 | 17 | 11 | 1.25 | 1.55 |
| V | 22 | 128 | 60 | 0.37 | 2.13 |
| Ni | 16 | 62 | 20 | 0.78 | 3.10 |
| Cu | 15 | 40 | 25 | 0.60 | 1.60 |
| Zn | 20 | 128 | 71 | 0.28 | 1.80 |
| Ga | 3 | 16 | 17 | 0.19 | 0.94 |
| As | 141 | 366 | 1.5 | 94 | 244 |
| Rb | 29 | 116 | 112 | 0.26 | 1.04 |
| Sr | 71 | 171 | 350 | 0.20 | 0.49 |
| Y | 15 | 33 | 22 | 0.66 | 1.50 |
| Zr | 31 | 108 | 190 | 0.16 | 0.57 |
| Nb | 3 | 13 | 25 | 0.13 | 0.52 |
| Mo | 9 | 11 | 1.5 | 5.80 | 7 |
| Ag | 1.24 | 0.21 | 0.05 | 24.8 | 4.20 |
| Sb | 2021 | 529 | 0.2 | 10105 | 2645 |
| Ba | 76 | 142 | 550 | 0.14 | 0.26 |
| La | 4 | 25 | 30 | 0.15 | 0.83 |
| Ce | 17 | 51 | 64 | 0.26 | 0.80 |
| Nd | 8 | 18 | 26 | 0.30 | 0.69 |
| Au | 1.33 | *** | 0.002 | 665 | |
| Tl | 18 | 21 | 0.75 | 24.5 | 28.0 |
| Pb | 7 | 10 | 20 | 0.37 | 0.50 |
| Th | 27 | 15 | 10.7 | 2.49 | 1.40 |

*argillically altered samples
**Taylor and McClennan 1985
***most samples <0.05 ppm

of the deposit. The production of dolomite by hydrothermal alteration may be difficult to distinguish from sedimentary dolomite, which is abundant in "unaltered" Chainman Shale and Simonson Dolomite. One obvious type of dolomite-stable alteration is sanded dolomite, a porous and friable dolomite that disintegrates into sand-size granules when handled (e.g., Lovering 1949). It occurs in discontinuous bodies, not more than 2 m in diameter, along the northwest-striking fault between the Simonson Dolomite and Chainman Shale and locally near calcite-filled cavities within otherwise unaltered Simonson Dolomite. Thin sections reveal that the sanded dolomite has a greater fraction of fine-grained noncarbonate and opaque minerals compared to unaltered dolomite and also contains veinlets of quartz. Sanded dolomite may represent recrystallization of sedimentary dolomite or, alternatively, dolomitization of minor limestone or calcite alteration products in the Simonson dolomite. The Ca/Mg ratio of the sanded dolomite is unchanged from the inferred precursor dolomite, and thus these rocks probably were not produced by simple dissolution of calcite in the original dolomitic rock. This rock is discussed further below. In addition, one argillic sample (GB-2) collected in the Chainman Shale contains much more dolomite (CaO + MgO 53 wt %) than a sample of its unaltered protolith (GB-63; 18 wt %). This also indicates that the hydrothermal fluids deposited dolomite locally.

Examples of the deposition of calcite by hydrothermal fluids are also present at Golden Butte, primarily in the Simonson Dolomite. Many cavities, 30 cm to 6 m in diameter, filled with coarse calcite are present within the apparently unaltered dolomite. These cavities appear to be related to hydrothermal fluids that flowed along joints and faults within the dolomite. Also, many coarse-grained calcite veins that cut the jasperoid in the Simonson Dolomite are present.

## GEOCHEMISTRY

### MASS TRANSFER

Comparisons of unaltered and altered Chainman Shale and Simonson Dolomite can be used to calculate gains and losses of materials needed to produce the resulting alteration products. For example, Jewell and Parry (1988) concluded that jasperoid facies rocks at Mercur, Utah, were derived by decarbonation of a silty limestone, without introduction of $SiO_2$. Here, we use a combination of "isocon diagrams" (Grant 1986) and Gresens' equation (1967) to show graphically and mathematically which elements were introduced or removed during the alteration process. An isocon diagram is an X-Y plot of concentrations of elements in an altered rock against those in the original rock. The immobile elements (those not added or removed) generate a straight line (an isocon) through the origin. The slope of the isocon shows the volume (or mass) change during alteration, and any deviation of an element from the isocon represents a concentration change. Moreover, there is no requirement that the alteration be pervasive; samples may be "mixtures" of variably altered rocks. For example, isocon analysis of a veined, but otherwise unaltered rock would reveal the composition of the vein-filling material and the proportion of veins. However, if two types of alteration occurred in one sample (e.g., veining followed by weathering), their compositions and proportions would not be separately recovered.

Figure 9 is an isocon diagram of average jasperoid from Golden Butte plotted against unaltered Chainman Shale (GB-63). A mean of 12 jasperoids from the Chainman Shale was calculated for 25 minor and trace elements and the major oxides as discussed above. A small number of anomalous values, 20 out of 420, were discarded because they would have heavily biased the averages. Sodium, Se,

*Table 5.—Comparison of Trace Element Concentrations in Golden Butte Jasperoid to Other Jasperoids in Carlin-Type Deposits* (ppm).*

| | Golden Butte (Mean) | Carlin (Mean) | Mercur (Mean) | Vantage (Mean) | Elephant Head (Mean) | Drum (Mean) | Great Basin (Geometric Mean) |
|---|---|---|---|---|---|---|---|
| Sc | 14 | 0 | | | | | |
| V | 22 | 70 | | | | | 20 |
| Ni | 16 | 3 | | | | | 12 |
| Cu | 15 | 70 | | | 76 | 3213 | 16 |
| Zn | 20 | 6 | | | 83 | 532 | 35 |
| Ga | 3 | 0 | | | | | |
| As | 141 | 385 | 842 | 280 | 212 | 566 | 220 |
| Rb | 29 | | | | | | |
| Sr | 71 | 10 | | | 182 | | 29 |
| Y | 15 | 0 | | | | | |
| Zr | 31 | 20 | | | | | |
| Nb | 3 | 0 | | | | | |
| Mo | 9 | 5 | | | | 18 | 7 |
| Ag | 1.2 | 1 | 0.13 | 3.3 | 4 | 3.5 | 0.7 |
| Sb | 2021 | 40 | 989 | 160 | 6 | 153 | 86 |
| Ba | 76 | 500 | | | 917 | | 307 |
| La | 5 | 0 | | | | | 5 |
| Ce | 17 | | | | | | |
| Nd | 8 | | | | | | |
| Au | 1.3 | 23 | 0.13 | 2 | | 2.6 | 0.2 |
| Tl | 18 | 0 | 47 | | 1 | | |
| Pb | 7 | 0 | | | 130 | 332 | 24 |
| Th | 27 | | | | | | 2 |

space = not analyzed

*Data from: Holland and others 1988, Ilchik 1990, Jewell and Parry 1988, Nutt and others 1991, Radtke and others 1980, Theodore and Jones 1992

and Bi were discarded because most of the concentrations were below detection limits. Because they are better estimates of bulk rock composition, only the concentrations of Cu and Zn analyzed by XRF were used. The average jasperoid composition, shown by the position of the element symbol and box and whisker plots, were plotted against the elemental concentrations in the unaltered Chainman Shale (fig. 9). Many concentrations have been scaled using an multiplication factor so symbols would not overlap (Wilson 1992).

Assuming aluminum was immobile during hydrothermal alteration (because of its low solubility in water), an isocon was drawn from the origin through Al. Other elements that are immobile in many hydrothermal environments, such as Ti, Zr, Ga, La, Nd, Nb, and Y, have ranges that easily overlap the isocon and justify using a constant aluminum isocon. The ranges of some other elements that are typically mobile, such as Pb, Mo, Mn, Fe, Rb, V, and K, also overlap the isocon. Elements that have been significantly enriched relative to the unaltered shale are found above the isocon and include Au, Ag, Hg, As, Sb, Tl, Cu, and Si. Elements lost were Ca, Mg, and S. The suite of trace elements enriched is similar to the pathfinder elements indicative of sediment-hosted, disseminated gold deposits. The addition of Si and the removal of Ca and Mg is due to silicification and carbonate removal during replacement. We do not think that the depletion of S is simply the result of destruction of alteration-produced sulfides during weathering. Many of the pieces of jasperoid analyzed show no signs of oxidation. Moreover, our samples of the Chainman Shale (1.8% S) were exposed to similar conditions of weathering without S depletion. Rather, we conclude that during jasperoid formation some sulfides became unstable in the parental carbonaceous shale; S concentrations were further lowered by dilution because other components, mainly silica, were introduced.

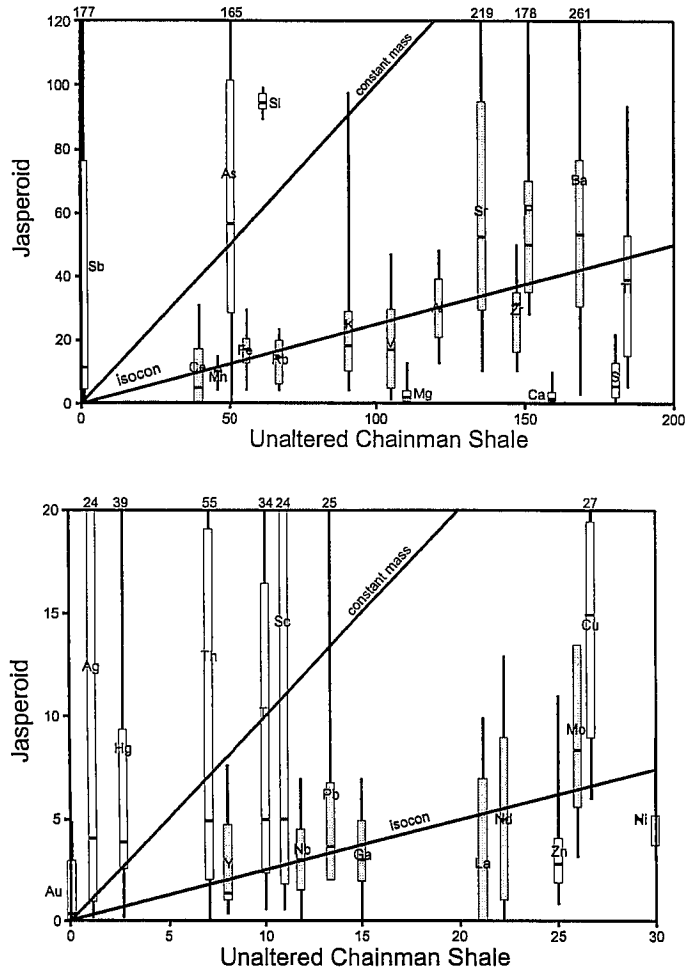


FIGURE 9.—*(a) Isocon diagram depicting relative concentrations of an average of 12 jasperoids versus unaltered Chainman Shale (GB-63). Element symbols are located at sample means, and the box (median, first, and second quartiles) and whisker (minimum and maximum values) symbols show the range of values, arbitrarily scaled to prevent overlap of the symbols. Shaded boxes represent elements that lie on or near the isocon. Maximum values outside the range of the diagram are shown at the top of the figure. (b) Isocon diagram of elements that appear near the origin of the graph in figure 9a. The slope of the isocon drawn through Al is 0.25.*

*Table 6.—Fraction of Elements Gained or Lost During Alteration.*

| | Fraction Gained or Lost (–) | | | |
|---|---|---|---|---|
| | Jasperoid (average) | Argillic (GB-9) | Argillic (GB-2) | Sanded Dolomite (GB-23) |
| Sc | 4.4 | 12.0 | | |
| V | –0.29 | 3.7 | –0.18 | 9.7 |
| Ni | –0.33 | –0.87 | 0.46 | 27.2 |
| Cu | 1.3 | 0.35 | –0.28 | –0.28 |
| Zn | –0.42 | –0.89 | 2.4 | 15.2 |
| Ga | –0.11 | 1.68 | –0.19 | |
| As | 4.59 | 11.8 | 1.9 | 7.5 |
| Rb | –0.21 | 0.15 | –0.17 | –0.01 |
| Sr | 1.9 | 0.36 | 1.7 | 0.12 |
| Y | 1.0 | 3.0 | –0.23 | 89.2 |
| Zr | –0.22 | 0.05 | –0.14 | –0.13 |
| Nb | 0.07 | 0.30 | 0.14 | –0.10 |
| Mo | 0.44 | –0.44 | –0.84 | 3.4 |
| Ag | 43.0 | 199 | –0.04 | 2.1 |
| Sb | 1770 | 4480 | 39.6 | 12.1 |
| Ba | 0.67 | 1.0 | –0.51 | 4.1 |
| La | –0.5 | –0.32 | –0.03 | |
| Ce | –0.01 | 1.5 | 0.75 | |
| Nd | –0.1 | –0.17 | –0.17 | 2.6 |
| Au | 245 | 638 | | 7.7 |
| Hg | 11.4 | 11.3 | 1.8 | 1.3 |
| Tl | 3.1 | 6.5 | 1.1 | 117 |
| Pb | 0.94 | 0.02 | –0.08 | 2.3 |
| Th | 6.3 | 27.9 | –0.26 | |
| $SiO_2$ | 5.1 | 0.37 | 0.02 | 2.3 |
| $TiO_2$ | –0.18 | –0.02 | –0.25 | |
| $Al_2O_3$ | 0 | 0 | 0 | 43.2 |
| $Fe_2O_3$ | 0.19 | 4.0 | 0.08 | 6.3 |
| MnO | –0.25 | –0.74 | 0.95 | 16.4 |
| MgO | –0.88 | –0.76 | 4.1 | –0.02 |
| CaO | –0.93 | –0.96 | 4.5 | 0 |
| $Na_2O$ | | 0.32 | | |
| $K_2O$ | 0.07 | 0.27 | –0.26 | 0.03 |
| $P_2O_5$ | 0.62 | 0.98 | 0.64 | 2.0 |
| S | –0.83 | –0.18 | | |

space = element in one or both samples below detection
*argillically altered sample

The slope of the isocon, approximately 0.25, indicates that a large amount of dilution due to a change (~300% added) in volume and/or mass occurred during silicification. Dilution of the immobile elements by the addition of a large volume of silica during alteration process is the most likely reason for the shallow isocon. In contrast, Ilchik (1991) concluded that replacement of carbonate with silica at the Vantage gold deposit was volume conservative, and Bakken (1991) suggested a 50% decrease in rock volume accompanied silicification at the Carlin deposit.

An estimate of the fraction of an element gained or lost during the creation of the jasperoid can be made using the slope of the isocon and Gresens' equation (1967) as described by Grant (1986). Table 6 lists the fraction gained or lost for each element analyzed. It is important to remember the fraction gained represents only the average of the 12 samples. Antimony concentrations changed the most during alteration, having increased over 1,700 times that of shale host. Gold increased over 200 times, Ag and Hg over 10 times, and Th, Si, As, Na, Sc, Tl, Sr, Cu, and Y

over 100%. Approximately 90% of the Ca and Mg, originally as dolomite, were removed during alteration.

These data indicate that the final alteration product was produced by the removal of most of the CaO and MgO (calcite and dolomite dissolution), which make up about 18 wt percent of the unaltered host, and the addition of $SiO_2$, which composes greater than 95 wt percent of the jasperoid. The jasperoid compositions at Golden Butte cannot be explained by simple carbonate removal from the host as suggested by Jewell and Parry (1988) for the Mercur, Utah, gold deposit. Silicification at Golden Butte could have occurred by replacement and by open-space filling in a highly porous host. Although some open space was probably created by carbonate dissolution, much of the porosity must have been created during multiple periods of faulting that took place prior to formation of the jasperoid. Subsequent brecciation of the jasperoid followed by precipitation of quartz in open spaces further diluted the immobile elements.

Figure 10 is an isocon diagram of unaltered Chainman Shale versus a sample containing an intimate mixture of jasperoid and argillically altered host (GB-9) collected from the Chainman Shale. Titanium, Zr, Nb, and Nd all fall on or very near an isocon drawn through Al, suggesting they were immobile during argillic alteration. The slope of this isocon is 0.77, demonstrating a smaller change in mass and/or volume during alteration than occurred in the jasperoid. The elements above and below the isocon are nearly identical to those in the jasperoids. In this case, $SiO_2$ has increased by 37%, and $Fe_2O_3$ has increased 400% (table 6). The Au (12.3 ppm) and $Fe_2O_3$ (21 wt %) concentrations in this sample are extremely high compared to the only other argillically altered Chainman Shale sample analyzed (GB-2) (fig. 11). GB-2 is a brecciated, argillically altered sample with a clay matrix. The most unusual aspect of GB-2 is the abundance of CaO and MgO (greater than 50 wt %) as dolomite, compared to the unaltered Chainman Shale (18 wt %). In this case, Ca, Mg, Mn, Zn, and Ni all fall above the isocon, rather than below, as in GB-9. It is possible that the circulating hydrothermal fluids were undersaturated with respect to dolomite, and thus removed Ca and Mg in some areas within the system. As physical and chemical conditions changed, the fluid may have become supersaturated with respect to dolomite, as outlined by Hofstra and others (1991). The slope of this isocon in figure 11 is 0.57, indicating a greater change in mass and/or volume than in sample GB-9. This change is probably the result of brecciation and the introduction of dolomite and minor sulfides hosting Sb, Zn, and Ni. Silica appears to have been "immobile" in this sample. The pathfinder elements As, Sb, Tl, and Hg have increased in concentration by 100% or greater in GB-2, although gold is below detection (table 6). The increase for each of the pathfinder elements was much less than in GB-9 and in the jasperoids.

Figure 12 is an isocon diagram for sanded dolomite (GB-23) collected along the northwest fault (fig. 6) and an apparently unaltered dolomite (GB-25) located about 9 m

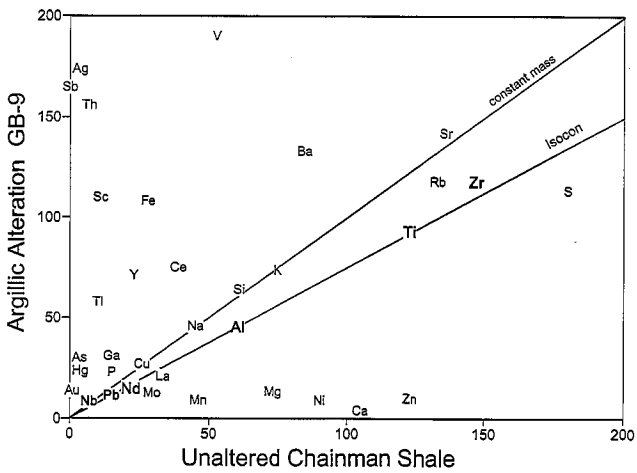


FIGURE 10.—*Isocon diagram, constructed as in figure 9, for an argillically altered sample (GB-9) of Chainman Shale versus unaltered Chainman Shale (GB-63). The occurrence of MgO and CaO below the constant aluminum isocon and Au with the other pathfinders above the isocon represent decarbonatization and mineralization. Bold letters represent elements that lie on or near the isocon.*

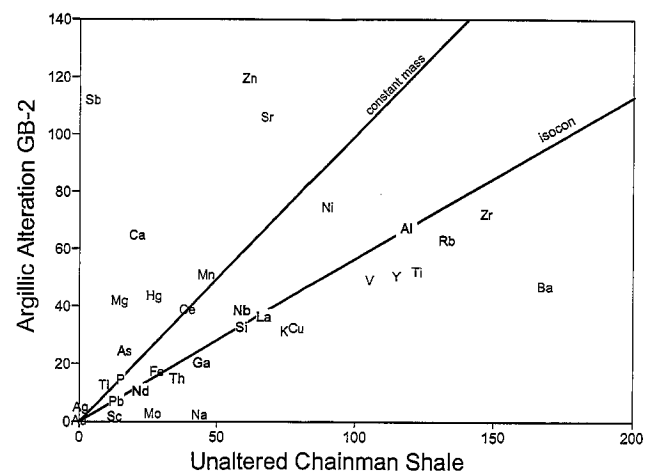


FIGURE 11.—*Isocon diagram, constructed as in figure 9, of an argillically altered sample GB-2 from the Chainman Shale versus unaltered Chainman Shale (GB-63). The addition of MgO and CaO indicate deposition of dolomite may have occurred in addition to mineralization during alteration. Bold letters represent elements that lie on or near the isocon.*

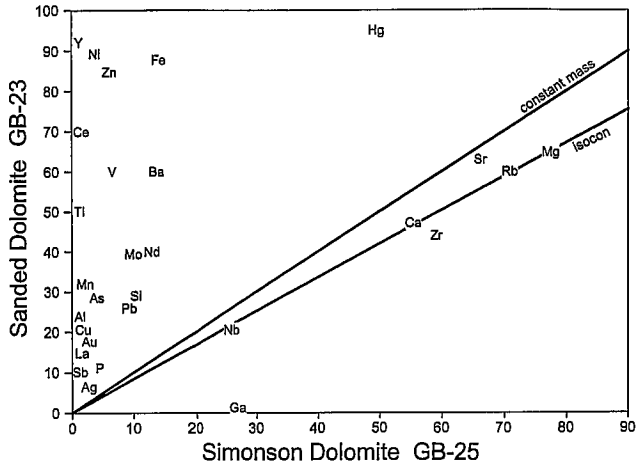


FIGURE 12.—*Isocon diagram, constructed as in figure 9, of sanded dolomite (GB-23) versus unaltered Simonson Dolomite sample located 9 meters away. Nearly all elements depicted fall near or above the "isocon," indicating their addition by hydrothermal fluids traveling up the fault.*

away. The composition of GB-25 is very similar to another sample of Simonson Dolomite (GB-62) collected 2 km from the pit. The $Al_2O_3$ concentration in the unaltered dolomite is so low that it cannot be used to define an isocon. The only elements to define a trend similar to an isocon include some "immobile" elements (Nb, Zr), as well as Ca, Sr, Rb, and Mg, but many of these occur in very low concentrations. Perhaps recrystallization took place under dolomite stable conditions, making mass transfer calculations difficult. However, it is clear that most of the elemental concentrations increased during alteration. The most notable increases include Si, Fe, Al, Au, Ag, As, Sb, Hg, Tl, Pb, Ba, Zn, and Ni (fig. 12, table 6). Enrichments were nonetheless quite small compared to those calculated for the jasperoid. Thin sections of the two samples show that the sanded dolomite has abundant opaque and fine-grained noncarbonate minerals and contains veinlets of quartz. The opaque grains apparently represent the Fe, Sb, Zn, and Ni minerals, and the fine-grained material may be clays that were introduced, perhaps mechanically, into the porous sanded dolomite by the hydrothermal fluids.

## STATISTICAL ANALYSIS

Frequency distributions of the trace-element concentrations in the samples from Golden Butte are strongly skewed positively; that is, the most frequently occurring values fall in the lowermost range of reported concentrations with the relatively few higher concentrations, forming a long "tail" in the distribution. By transforming the concentrations to base 10 logarithms, the distributions of the elements tend to form more normal distributions. Data with normal distributions are more useful when performing standard statistical calculations. However, histograms of Bi, Se, and Cd are still strongly skewed positively because most of the concentrations are below detection limits. Therefore, these elements were eliminated from the statistical analysis.

To examine chemical variations within the major rock types at Golden Butte, data were separated into three groups: jasperoids, argillic rocks (including carbonaceous types), and dolomites (including GB-27 that is primarily

*Table 7.—Summary of Geochemical Data for Jasperoid Samples.*

| | No. Samples | Geometric Mean | Geometric Deviation | Low Value | High Value |
|---|---|---|---|---|---|
| Sc* | 14 | 10 | 5.1 | 1 | 177 |
| V | 14 | 17 | 3.5 | 1 | 221 |
| Ni | 14 | 15 | 1.4 | 9 | 28 |
| Cu-xrf | 14 | 13 | 1.7 | 5 | 27 |
| Cu-icp | 32 | 8 | 2.5 | 0 | 28 |
| Zn-xrf | 14 | 19 | 2.5 | 4 | 187 |
| Zn-icp | 32 | 19 | 3.3 | 2 | 280 |
| Ga | 13 | 3 | 2.6 | 0 | 7 |
| As | 32 | 135 | 3.2 | 4 | 2510 |
| Rb | 14 | 27 | 2.5 | 5 | 196 |
| Sr | 14 | 60 | 2.8 | 10 | 488 |
| Y | 14 | 7 | 3.4 | 1 | 52 |
| Zr | 14 | 27 | 1.7 | 10 | 69 |
| Nb | 14 | 2 | 2.3 | 0 | 7 |
| Mo | 32 | 9 | 2.1 | 2 | 50 |
| Ag | 32 | 0.70 | 5.9 | 0.01 | 58 |
| Sb | 32 | 1426 | 11.6 | 0 | 96000 |
| Ba | 14 | 122 | 11.8 | 3 | 162531 |
| La | 7 | 10 | 3.7 | 1 | 94 |
| Ce | 11 | 16 | 4.0 | 1 | 152 |
| Nd | 12 | 6 | 2.7 | 1 | 41 |
| Au | 32 | 0.297 | 5.37 | 0.025 | 4.87 |
| Hg | 32 | 6 | 3.8 | 0 | 185 |
| Tl | 32 | 8 | 3.5 | 1 | 128 |
| Pb | 32 | 5 | 3.2 | 1 | 128 |
| Th | 12 | 13 | 4.6 | 2 | 197 |
| $SiO_2$** | 14 | 88.5 | 1.16 | 58.2 | 99.1 |
| $TiO_2$ | 14 | 0.09 | 2.60 | 0.01 | 0.32 |
| $Al_2O_3$ | 14 | 2.73 | 1.51 | 1.27 | 4.86 |
| $Fe_2O_3$ | 14 | 1.41 | 1.66 | 0.41 | 2.95 |
| MnO | 14 | 0.01 | 1.54 | 0.00 | 0.02 |
| MgO | 14 | 0.21 | 2.94 | 0.02 | 1.27 |
| CaO | 13 | 0.26 | 5.23 | 0.06 | 17.89 |
| $Na_2O$ | 14 | 0.03 | 2.27 | 0.01 | 0.13 |
| $K_2O$ | 14 | 0.56 | 2.32 | 0.13 | 3.26 |
| $P_2O_5$ | 14 | 0.05 | 1.56 | 0.03 | 0.18 |
| S | 12 | 0.05 | 7.33 | 0.00 | 2.05 |

*Sc to Th ppm
**$SiO_2$ to S wt%

*Table 8.—Summary of Geochemical Data for Argillically Altered Samples (ppm).*

| | No. Samples | Geometric Mean | Geometric Deviation | Low Value | High Value |
|---|---|---|---|---|---|
| Cu | 28 | 13 | 2.4 | 2 | 92 |
| Zn | 28 | 25 | 4.3 | 3 | 2650 |
| As | 28 | 197 | 4.2 | 7 | 1731 |
| Mo | 28 | 8 | 3.6 | 0 | 45 |
| Ag | 28 | 0.13 | 3.85 | 0.01 | 17.4 |
| Sb | 28 | 173 | 6.6 | 5 | 16700 |
| Au | 28 | 0.053 | 4.15 | 0.025 | 12.3 |
| Hg | 28 | 4 | 4.4 | 0 | 50 |
| Tl | 28 | 7 | 4.4 | 1 | 424 |
| Pb | 28 | 9 | 3 | 0 | 43 |

*Table 9.—Summary of Geochemical Data for Dolomites (ppm).*

| Variable | No. Samples | Geometric Mean | Geometric Deviation | Low Value | High Value |
|---|---|---|---|---|---|
| Cu | 12 | 2 | 3.1 | 0 | 18 |
| Zn | 12 | 13 | 6.2 | 1 | 427 |
| As | 12 | 12 | 4.5 | 1 | 181 |
| Mo | 12 | 1 | 3.7 | 0 | 14 |
| Ag | 12 | 0.09 | 3.86 | 0.02 | 2.74 |
| Sb | 12 | 77 | 10.9 | 0 | 7593 |
| Au | 12 | 0.050 | 2.73 | 0.025 | 0.48 |
| Hg | 12 | 1 | 3.9 | 0 | 22 |
| Tl | 12 | 3 | 4.3 | 0 | 50 |
| Pb | 12 | 1 | 2.3 | 0 | 6 |

calcite). Summary statistics of the geochemical data for each sample type are given in tables 7 to 9.

Principal component analysis, using the computer program SAS (Statistical Analysis Systems 1988), was used to detect significant element associations in each alteration type. The logarithmically transformed ICP data for the three types of rocks were scaled to decimal fractions of their ranges so that the elements with relatively high or low concentrations would not dominate the results. The combined XRF and ICP analysis of the jasperoid samples were examined separately. Table 10 lists the factors in order of decreasing factor score for each rock type. Only factors that account for 5% or greater of the variance are listed; elements are shown in order of decreasing factor score (greater than 0.2). Principal component analysis using the ICP data for all three rock types shows that most elements are heavily loaded into factor 1. This factor apparently reflects the introduction of pathfinder elements that typically are associated with Carlin-type deposits.

In the jasperoids and the argillic rocks, Au and Ag have the heaviest loading in factor 2. Silver and gold are found in factor 3 in the dolomite, and this factor accounts for a smaller percent of the variance. This is because concentrations of gold in 10 of the 12 dolomite samples are below detection limits, and Ag concentrations are generally low. Principal component analysis performed by Theodore and Jones (1992) on a gold-bearing jasperoid near Battle Mountain, Nevada, and factor analysis performed by Holland and others (1988) on mineralized and nonmineralized jasperoids samples collected throughout the Great Basin have Au, Ag, Sb, Pb, and As in a single factor interpreted as the mineralization factor. The strong loading of Au and Ag into a separate factor for gold-mineralized Golden Butte rocks could be interpreted as evidence that the precious metals were deposited from fluids unrelated to the fluid that carried the pathfinder elements. Alternatively, and more likely considering the strong spatial association, the chemistry of the same hydrothermal fluids that deposited the pathfinders may have changed enough to allow Au and Ag to become saturated and precipitate separately in time or space from the pathfinders. For example, Wood and others (1987) have measured the solubilities of pyrite, pyrrhotite, magnetite, sphalerite, galena, gold, stibnite, bismuthinite, argentite, and molybdenite in a chloride-free solution from 200° to 350°C at $CO_2$ partial pressures from 0.69 to 172 bars with oxygen and sulfur fugacities controlled by the pyrite-pyrrhotite-magnetite buffer. Under this range of conditions the relative solubilities are Sb > Fe > Zn > Pb > Ag, Mo > Au, Bi. If deposition of Au and Ag occurred under similar conditions at Golden Butte, the partitioning of Au-Ag and Sb-Zn-Pb into different factors may be explained by the solubility differences. Mo, Bi, and, to a lesser extent, Pb have not been enriched significantly in the altered rock at Golden Butte. These elements may not have been present in significant amounts in the hydrothermal fluids. Moreover, the distribution of gold mineralization is highly localized next to the faults (fig. 5) in the mine, whereas the alteration assemblages and pathfinder mineralization are much more extensive. The hydrothermal fluids could have deposited the less-soluble precious metals first, adjacent to the feeder zones, and the other pathfinder elements later and over a wider area.

The element associations in other factors listed are not as clearly defined or as easily interpreted and may represent other minor periods of mineralization or lateral changes in hydrothermal fluid chemistry.

Principal component analysis of the 14 jasperoid samples analyzed by XRF and ICP indicates that a five-factor model accounts for about 82% of the variance in the geochemical data (table 11). Factor 1 is interpreted as representing mineralization not related to gold deposition. The pathfinder elements Sb and Tl, as well as Ba, are in this

*Table 10.—Element Associations in ICP Analyses of Major Rock Types at Golden Butte.*

| Factor Number | Element association (in order of decreasing factor score) | Percent of Variance |
|---|---|---|
| Jasperoid | n = 32 | |
| 1 | As, Zn, Mo, Hg, Au, Tl, Sb, Cu, Pb | 38.2 |
| 2 | Ag, Au, Cu | 17.3 |
| 3 | Tl, Ag, Sb, Au | 15.1 |
| 4 | Pb, Sb, Zn | 10.9 |
| 5 | Cu, Tl, Zn | 7.7 |
| Argillic | n = 28 | |
| 1 | As, Hg, Cu, Mo, Sb, Pb, Tl, Ag | 40.8 |
| 2 | Au, Ag, Sb, Hg | 21.9 |
| 3 | Zn, Tl, Cu | 11.6 |
| 4 | Ag, Au, As, Cu, Mo | 7.3 |
| 5 | As, Mo, Sb, Zn | 5.9 |
| Dolomite | n = 12 | |
| 1 | Hg, Mo, As, Cu, Au, Pb, Tl, Zn, Ag | 66.8 |
| 2 | Sb, Zn, Tl | 11.9 |
| 3 | Ag, Tl, Au | 9.3 |
| 4 | Sb, Hg, Pb | 5.0 |

Jasperoid: samples consisting primarily of quartz
Argillic: samples consisting primarily of clay
Dolomite: samples consisting primarily of dolomite

*Table 11.—Element Associations and Synoptic Interpretation of XRF Analyses of Jasperoids at Golden Butte.*

| Factor Number | | Element association (in order of decreasing absolute value of the factor score) | Percent of Variance |
|---|---|---|---|
| 1 | (+) | Sb, Th, Sc, Tl, Y, Ba | 23.6 |
| | (–) | $SiO_2$, Cu, Rb, Ga, Nb | |
| 2 | (+) | $TiO_2$, Zr, V, Pb, Ce, $Fe_2O_3$, $Al_2O_3$, As, $P_2O_5$, Nb | 22.1 |
| 3 | (+) | MgO, $K_2O$, Rb, $Al_2O_3$, CaO | 15.5 |
| | (–) | As, $Al_2O_3$, Mo, Hg | |
| 4 | (+) | MnO, Ni, Zn, Ce, Tl, Au, Ag | 11.5 |
| | (–) | Nd, Sr | |
| 5 | (+) | Au, Ag, $Na_2O$ | 9.4 |
| | (–) | CaO, La, MgO, Zr, La | |
| | | Interpretation | |
| 1 | | Non-Au related mineralization | |
| 2 | | Residuum of immobile elements | |
| 3 | | Remnants from argillic components | |
| 4 | | Uncertain | |
| 5 | | Precious metal mineralization | |

factor. Thorium and Sc are also loaded in this factor. These two elements, not commonly determined by exploration programs, have not been previously reported as present in anomalous amounts in other sediment-hosted disseminated gold deposits, but examination of the geochemical data (table 1) and isocon diagrams shows that both elements have concentrations in the jasperoid commonly much greater than that of unaltered Chainman Shale and Simonson Dolomite. Therefore, Th and Sc may have been introduced by the same mineralizing fluids as the traditional pathfinders. Gold and Ag have negative factor loadings, so this factor may imply that jasperoid became enriched in pathfinders during a stage of mineralization barren in precious metals or jasperoid formed in an area where the ore fluid did not precipitate appreciable Au and Ag.

Factor 2 has high loadings in the generally immobile elements $TiO_2$, Zr, Ce, $Al_2O_3$, and Nb. Also, V, Pb, and $Fe_2O_3$, which overlap the jasperoid isocon in figure 9, have high scores for this factor. Consequently, this factor is interpreted as the residuum from the original host that has been diluted by introduction of $SiO_2$ but not removed during the alteration process.

Factor 3, with high scores in MgO, $K_2O$, $Al_2O_3$, and CaO, contains high loadings for the major constituents of the Chainman Shale protolith. Factor 3 may represent the carbonate and clay constituents of the original host rock. Alternatively, this factor might represent argillic alteration (high $K_2O$ and $Al_2O_3$) or precipitation of hydrothermal dolomite or calcite (high MgO and CaO).

Factor 4 has relatively high scores for the first row transition metals Mn, Ni, and Zn. MnO variations, however, may not be meaningful because the concentrations range between < 0.01 and 0.02 wt percent, well within the error of the XRF technique (±0.01 to 0.02%). This component is the least understood of the five factors. The presence of Au and Ag in this factor suggests that weak gold mineralization is related to enrichments of transition metals in some jasperoid samples.

The precious metals Ag and Au have the highest scores in factor 5. This factor is interpreted as related to precious metal mineralization similar to that described in factor 2 derived from principal component analysis of the ICP data for argillic and jasperoid samples.

## FLUID INCLUSION STUDY

Fluid inclusions in five jasperoid samples representing a range of gold concentrations and textures were studied.

Two types of fluid inclusions were identified. Type 1 inclusions are liquid-rich with vapor bubbles occupying 5% to 40% of the total volume of the inclusion and no daughter minerals. Type 2 inclusions contain three phases—liquid $H_2O$, liquid $CO_2$, and $H_2O$-$CO_2$ vapor. Only one example of this inclusion type was found in a late barite vein. Many secondary fluid inclusions, located on healed fracture planes, are present in all samples examined. These inclusions are always less than 5 microns in diameter and thus not usable for freezing and heating measurements.

The samples and locations of fluid inclusions studied were:

CP-2—groundmass quartz in jasperoid with highly variable quartz grain sizes and abundant larger quartz crystals (> 1 mm) (Au = 0.617 ppm),

CP2-3—quartz in coarse and highly variable-sized quartz grains in groundmass and in filled or partially filled vugs (Au = 2.69 ppm),

CP-6—extremely coarse quartz (up to 1 cm in diameter) in vein cutting a fine-grained brecciated jasperoid (Au < 0.05 ppm),

GB-35—coarse barite from veins in a fine-grained jasperoid (Au = 0.33 ppm),

GB-29—a single cleavage fragment of calcite from a vein in jasperoid (Au = 0.093 ppm).

In general, primary fluid inclusions in the jasperoid matrix (quartz not related to veins) were small and not abundant. Only 14 such inclusions were usable for measuring freezing points in samples CP-2 (7 inclusions) and CP2-3 (7 inclusions), and homogenization temperatures were obtained for only 11 of these. The inclusions in the jasperoid matrix ranged between 6 and 15 microns along their longest dimension. Fluid inclusions in the coarse quartz (CP-6) and barite veins (GB-35) were large (15 to 60 microns) and relatively abundant; 57 inclusions were studied. No usable fluid inclusions were found outside of the veins in samples CP-6 and GB-35. Three relatively large fluid inclusions (0.03–1.2 mm) were examined in the calcite vein (GB-29).

## HOMOGENIZATION TEMPERATURES AND FLUID SALINITIES

Salinities of the type 1 fluid inclusions were estimated using the equation of Potter and others (1978). The approximate salinity of the type 2 inclusion was calculated with the equation of Bozzo and others (1975). Where inclusions were abundant (samples CP-6 and GB-35), all freezing data were collected prior to the heating runs. In samples with rare usable fluid inclusions (samples CP-2 and CP2-3), freezing and heating data were collected in succession for each inclusion.

Temperatures of homogenization in quartz from the three jasperoid samples range between 135° and 295°C,

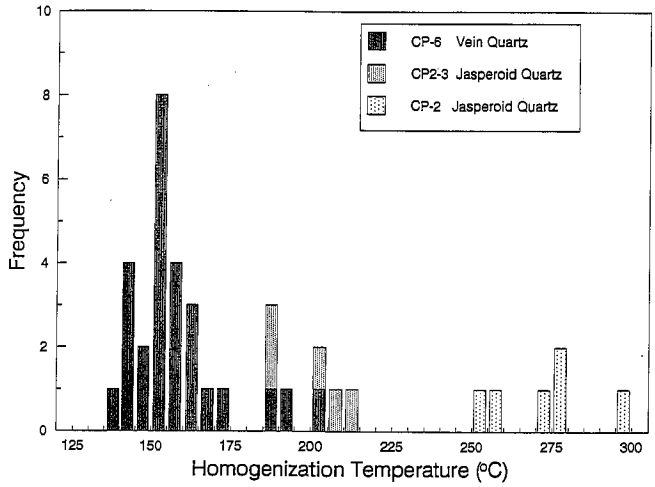


FIGURE 13.—*Histogram of fluid inclusion homogenization temperatures in quartz from three jasperoid samples.*

but individual samples have much narrower ranges (fig. 13). The highest temperature mode is produced by inclusions in matrix quartz from CP2-3 with a range of 250° to 295°C. A mid-temperature mode is formed by inclusions in matrix quartz from CP-2 from 185° to 210°C. Homogenization temperatures in the quartz veins of sample CP-6 range between 135° and 200°C with a mode at 145°C.

Heating experiments performed on the barite vein were not used because of the nonreproducibility of the homogenization temperatures caused by inclusion stretching during the heating experiments. Two heating measurements on the first inclusion examined in the barite vein (GB-35) showed an increase from 170° to 238°C. Homogenization temperatures of other fluid inclusions from the same chip ranged from 147° to 325°C with repeated measurements on individual inclusions showing systematic increases in homogenization temperatures. The first heating measurement taken on the barite (170°C), presumably when the least amount of stretching occurred, must represent a maximum homogenization temperature. Also because of problems with stretching, no homogenization temperatures were measured on inclusions in the vein calcite (GB-29).

Salinities of the fluid inclusions in jasperoid are low, ranging from 0 to 6 wt percent NaCl equiv. Salinities of the inclusions from each sample show more overlap than the temperatures of homogenization (fig. 14). The fluid inclusions with the highest salinities (4.5–6 wt % NaCl equiv) were found in the quartz vein in jasperoid CP-6. Vein barite in GB-35, vein calcite in GB-29, and jasperoid quartz in CP-2 have salinities close to zero, and quartz in

CP2-3 has intermediate salinity (< 3 wt percent NaCl equiv). The single type 2 fluid inclusion in barite (GB-35) exhibited an unusually high salinity of 12 wt percent NaCl equiv.

## INTERPRETATION OF FLUID INCLUSION DATA

Fluid inclusion analysis reveals that hydrothermal fluids poor in carbon dioxide and differing in temperature and salinity formed the gold-mineralized jasperoids and the quartz, barite, and calcite vein deposits at Golden Butte. No evidence of boiling was found with the fluid inclusions examined.

It is unlikely that the fluids that produced late quartz, barite, and calcite veins, such as in samples GB-6, GB-35, GB-29, are related directly to gold mineralization. We conclude this because gold concentrations in the vein-poor samples (CP-2 and CP-2-3) are higher than in the veined samples. Moreover, veining is pervasive throughout the jasperoids in the mine, whereas the highest gold grade is controlled by the position of the high-angle faults. Thus, the salinities (1–4 wt % NaCl equiv) and homogenization temperatures (185°–295°C) of fluid inclusions in the matrix of jasperoids CP-2 and CP2-3, though limited in number of measurements, are probably more representative of the ore-forming fluids. Temperature corrections (Roedder 1984) for these homogenization temperatures, assuming the depth of formation of jasperoid is around 1 to 2 km (as estimated by Seedorf 1991), are 20° to 40°C.

Matrix quartz in sample CP2-3 has fluid inclusion homogenization temperatures that overlap the range found in the jasperoid facies rocks at Mercur (220°–270°C) (Jewell and Parry 1988). Homogenization temperatures of sample CP-2 (180°–210°C) are lower but similar to those of fluid inclusions (in quartz, barite, calcite, sphalerite, and realgar) attributed to the main stage of mineralization at Carlin (175°–200°C) (Kuehn 1989, Radtke and others 1980). Ilchik (1991) reports limited fluid inclusion homogenization temperatures for calcite at the Vantage deposit were also between 190° and 250°C. Salinities in the fluids trapped in Golden Butte jasperoids were 1.5 to 4 wt percent NaCl equiv and similar to main mineralizing stage at Carlin (< 4 wt % NaCl equiv). Salinities of fluid inclusions in jasperoid facies rocks at Mercur were generally higher (5–8 wt % NaCl equiv) than any fluid inclusion examined in jasperoid or vein materials at Golden Butte. The temperatures of the fluids that produced the late veins at Golden Butte were 80° to 100°C lower than the main stage jasperoids, if vein quartz (CP-6) is representative. The salinities of most fluid inclusions in the quartz veins were 4 to 6 wt percent lower than those that formed the barite and calcite veins and may be related to different episodes of veining.

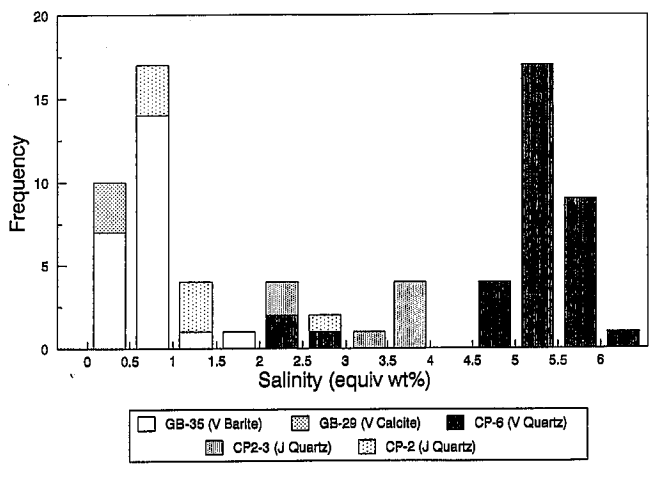


FIGURE 14.—*Histogram of fluid inclusion salinities in quartz, barite, and calcite veins and jasperoid quartz from five jasperoid samples.*

## DISCUSSION

### CONTROLS OF ALTERATION AND MINERALIZATION

The mineralization and alteration assemblages at Golden Butte show definite stratigraphic and structural controls. The alteration and distribution of gold ore is almost entirely restricted to the Chainman Shale. This unit is carbonate-poor and clay-rich compared to the silty carbonates that are the hosts of most Carlin-type gold deposits. It seems, therefore, that physical, rather than just chemical, properties of the Chainman Shale caused it to be more receptive to alteration and mineralization. Multiple periods of low-angle faulting may have produced zones of high permeability in the incompetent Chainman Shale. Later high-angle faults created avenues for the hypogene hydrothermal fluids to travel and collect between the two less permeable or unreactive dolomite units. These hydrothermal fluids dissolved carbonate and deposited silica (as jasperoid), Au, Ag, Sb, As, Tl, Sc, and Th in a zone paralleling the two high-angle normal faults, but restricted primarily to the more receptive Chainman Shale. The extent of ore grade gold mineralization (fig. 5) roughly follows the outline of this main jasperoid body.

Outward from the high-angle faults, the presumed feeders of the hydrothermal fluids, the deposit is crudely zoned from jasperoid to carbonaceous argillic rocks to zones in which dolomite was stable. Such zonation has been noted at other disseminated gold deposits, including Jerritt Canyon (Hofstra and others 1991).

*Fluid Thermometry and Chemistry*

The few homogenization temperatures obtained from fluid inclusions in jasperoid quartz grains range from 180° to 295°C. Salinities, in these inclusions, are low and have a narrow range (< 3.5 wt % NaCl equiv). The preservation of pyrite and organic carbon in unoxidized parts of the deposit indicates that the ore fluid was, at least initially, moderately reduced with gold probably transported as bisulfide complexes (Wood and others 1987). General lower salinities and temperatures obtained from fluid inclusions in two veined samples (one filled with quartz, the other barite) and mineral paragenesis (jasperoid quartz-pyrite-stibnite, coarse vein quartz, quartz-barite veins, stibiconite-limonite-barite-quartz in vuggy oxidized masses, calcite in veins and irregular masses) show that veining occurred during multiple periods of hypogene and/or supergene mineralization following jasperoid formation and involved cooler, relatively more oxidized fluids that ranged from 0–6 wt percent NaCl equiv.

Comparing the geochemistry of the unaltered and altered host rock helped delineate the composition of the hydrothermal fluids, the extent of metasomatism, and the role of replacement. Isocon diagrams of several alteration types show consistently the addition of $SiO_2$ (up to 5 times) and the trace-element assemblage commonly called pathfinders (maximum enrichments: Au = 640, Ag = 200, Sb = 4500, As = 12, Tl = 6, and Hg = 11) as well as Sc (up to 12 times) and Th (up to 28 times) (table 6). The deposition of anomalous amounts of the pathfinder elements shows that Golden Butte is similar to other Carlin-type deposits.

Principal component analysis revealed that high concentrations of As, Sb, Tl, and Hg correlate with each other but only weakly with Au and Ag. Also, areas of anomalous As, Sb, Tl, and Hg concentrations are extensive throughout the pit, whereas high grade gold mineralization is restricted to a zone close to the intersection of two high-angle faults. These observations may be explained by the differing solubilities of the elements in the hydrothermal fluids.

*Summary of Events*

Based on our observations, the sequence of events that produced the alteration and mineralization at Golden Butte was (1) low-angle faulting of the Simonson Dolomite placed the strongly deformed Chainman Shale between two relatively unreactive or impermeable units, (2) high-angle faulting further increased the permeability of the Chainman Shale and created channel ways for rising fluids, (3) massive influx of gold-bearing hydrothermal solutions from greater depths with temperatures of 180° to 295°C (uncorrected) and salinities of less than 4 wt percent NaCl equiv produced the jasperoid, argillic, and dolomitic alteration assemblages and deposited gold and other trace elements in anomalous amounts as sulfide minerals formed, (4) brecciation and further alteration occurred concurrent to and after this initial stage of mineralization, (5) reactions with cooler (Th < 175°C), more oxidizing hypogene fluids filled veins with quartz, barite, and calcite, and (6) supergene weathering and oxidation produced iron oxides, stibiconite from sulfides, more barite, and destroyed organic carbon. Sulfuric acid formed by the oxidation of sulfide converted sedimentary illites to kaolinite and alunite.

*Origin of Ore-Forming Hydrothermal Fluids*

Recently, it has been suggested that in some Carlin-type deposits gold was contributed by hydrothermal fluids convecting around igneous intrusions and deposited 5 or more kilometers from intrusion-centered base and precious metal districts (Sillitoe and Bonham 1990). The nearest known porphyry sulfide system (Butte Valley porphyry, Welsh and Miller 1990) to Golden Butte lies 11 km southwest. Moreover, aeromagnetic highs immediately west of the mine have been interpreted as buried intrusions. Thus, an igneous origin of the gold and/or hydrothermal fluid may be considered. However, the aeromagnetic highs near the deposit lie directly over, and are probably produced by, middle Tertiary volcanic rocks that lack a local intrusive system. Moreover, the ages of most porphyry systems in eastern Nevada are either Cretaceous or middle Tertiary. If our interpretation of the age of the deposit as late Tertiary is correct, then Au mineralization at Golden Butte and the porphyry system did not form at the same time. Without radiometric ages for the intrusion or better age constraints on the age of the gold deposit, an igneous origin of the hydrothermal system cannot be excluded with certainty. However, the Golden Butte deposit does not show the enhanced base-metal (Cu, Zn, Pb, Mo) concentrations found in jasperoid of the Drum, Utah (Nutt and others 1991), and Elephant Head, Nevada, deposits (Theodore and Jones 1992), which appear to be related to nearby intrusions.

Alternatively, the hydrothermal fluids that produced the Golden Butte deposit and other sediment-hosted gold deposits may have formed in response to late Tertiary extensional faulting and consequent deep circulation of groundwater that scavenged gold and other elements from sedimentary rocks and redeposited them (e.g., Hofstra and others 1991, Romberger 1986, Seedorff 1991). Carlin-type deposits would thus be unrelated to igneous activity. The two most-often stated reasons for this conclusion are (1) lack of field evidence linking deposits to igneous intrusions, and (2) oxygen and sulfur isotopic data that suggest that fluids are highly evolved meteoric waters containing

sulfur scavenged from Paleozoic sedimentary rocks (Hofstra and others 1991, Ilchik 1990, Radtke and Dickson 1974). This is our favored interpretation, but further data, especially stable isotopic data, are required to confirm it.

## ACKNOWLEDGMENTS

Alta Gold Company provided financial and logistical support for this project. Richard Hasler suggested this study, and Dana Durgin and Jack Sowers (all from Alta Gold Company) helped with the fieldwork and provided access to earlier results of mapping, drilling, and geochemical analyses. Theron Blatter and Kim Sullivan helped with computer applications. The comments of B. J. Kowallis, J. D. Keith, M. G. Best, C. E. Seedorf, and A. H. Hofstra were especially helpful.

## REFERENCES CITED

Armstrong, R. L., 1970, K-Ar dating using neutron activation for Ar analysis-comparison with isotope dilution Ar analysis: Geochimica et Cosmochimica Acta, v. 34, p. 233–36.

Bakken, B. M., 1991, Gold mineralization, wall-rock alteration, and the geochemical evolution of the hydrothermal system in the Main ore body, Carlin mine, Nevada: In Raines, G. L., Lisle, R. E., Schafer, R. W., and Wilkinson, W. H. (eds.), Geology and ore deposits of the Great Basin: Geological Society of Nevada, p. 233–34.

Bakken, B. M., and Einaudi, M. T., 1986, Spatial and temporal relations between wall rock alteration and gold mineralization, main pit, Carlin gold mine, Nevada, U.S.A.: In Macdonald, A. J. (ed.), Proceedings of Gold '86, an international symposium on the geology of gold: Toronto, p. 388–403.

Berger, B. R., 1986, Descriptive model of carbonate-hosted Au-Ag: In Cox, D. P., and Singer, D. A. (eds.), Mineral deposit models: U.S. Geological Survey Bulletin 1693, p. 175–77.

Bozzo, A. T., Chen, H. S., Kass, J. R., and Barduhn, A. J., 1975, The properties of the hydrates of chlorine and carbon dioxide: Desalination, v. 16, p. 303–20.

Carden, J. R., 1991, The discovery and geology of the Nighthawk Ridge deposit at Easy Junior, White Pine County, Nevada: In Raines, G. L., Lisle, R. E., Schafer, R. W., and Wilkinson, W. H. (eds.), Geology and ore deposits of the Great Basin: Geological Society of Nevada, p. 665–76.

Fritz, W. H., 1968, Geologic map and sections of the southern Cherry Creek and northern Egan Ranges, White Pine County, Nevada: Nevada Bureau of Mines Map 35, scale 1:62,500.

Gans, P. B., 1982, Multiple intrusion and faulting in the Hunter district, White Pine County, Nevada: M.S. thesis, Stanford University, 179p.

Gans, P. B., Mahood, G. A., and Schermer, E., 1989, Synextensional magmatism in the Basin and Range Province: A case study from the eastern Great Basin: Special Paper Geological Society America, v. 233, 58p.

Grant, J. A., 1986, The isocon diagram—A simple solution to Gresens' equation for metasomatic alteration: Economic Geology, v. 81, p. 1976–82.

Gresens, R. L., 1967, Composition-volume relationships of metasomatism: Chemical Geology, v. 2, p. 47–55.

Hasler, R. W., 1985, Butte project geologic report 1985: Amselco Exploration Inc., unpublished report, 18p.

Hofstra, A. H., Leventhal, J. S., Northrop, H. R., Landis, G. P., Rye, R. O., Birak, D. J., and Dahl, A. R., 1991, Genesis of sediment-hosted disseminated-gold deposits by fluid mixing and sulfidization: Chemical-reaction-path modeling of ore-deposition processes documented in the Jerritt Canyon district, Nevada: Geology, v. 19, p. 36–40.

Holland, P. T., Beaty, D. W., and Snow, G. G., 1988, Comparative elemental and oxygen isotope geochemistry of jasperoid in the northern Great Basin: Evidence for distinctive fluid evolution in gold-producing hydrothermal systems: Economic Geology, v. 83, p. 1401–23.

Hose, R. K., and Blake, M. C., Jr., 1976, Geology and mineral resources of White Pine County, Nevada, part 1: Nevada Bureau of Mines and Geology Bulletin 85, 35p.

Ilchik, R. P., 1990, Geology and geochemistry of the Vantage gold deposits, Alligator Ridge–Bald Mountain mining district, Nevada: Economic Geology, v. 85, p. 50–75.

_____, 1991, Geology of the Vantage gold deposits, Alligator Ridge, Nevada: In Raines, G. L., Lisle, R. E., Schafer, R. W., and Wilkinson, W. H. (eds.), Geology and ore deposits of the Great Basin: Geological Society of Nevada, p. 645–63.

Jewell, P. W., and Parry, W. T., 1988, Geochemistry of the Mercur gold deposit (Utah, U.S.A.): Chem. Geology, v. 69, p. 245–65.

Kuehn, C. A., 1989, Studies of disseminated gold deposits near Carlin, Nevada: Evidence for a deep geologic setting of ore formation: Ph.D. thesis, Pennsylvania State University, 395p.

Lovering, T. S., 1949, Rock alteration as a guide to ore—East Tintic district, Utah: Economic Geology Mon. 1, 65p.

_____, 1972, Jasperoid in the United States—Its characteristics, origin, and economic significance: U.S. Geological Survey Professional Paper 710, 164p.

Meyer, C., and Hemley, J. J., 1967, Wall rock alteration: In Barnes, H. L. (ed.), Geochemistry of hydrothermal ore deposits: New York, Holt, Rinehart, and Winston, p. 166–235.

Miller, R. D., 1971, Progress report Butte Valley–Cyprus examination: Bear Creek Mining Company, Intermountain District, Spokane, Washington, unpublished report, 21p.

Norrish, K., and Hutton, J. T., 1969, An accurate X-ray spectrographic method for analysis of a wide range of geological samples: Geochimica et Cosmochimica Acta, v. 33, p. 431–53.

Nutt, C. J., Thorman, C. H., Zimbelman, D. R., and Gloyn, R. W., 1991, Geologic setting and trace-element geochemistry of the Detroit mining district and Drum gold mine, Drum Mountains, west central Utah: In Raines, G. L., Lisle, R. E., Schafer, R. W., and Wilkinson, W. H. (eds.), Geology and ore deposits of the Great Basin: Geological Society of Nevada, p. 491–509.

Osmond, J. C., 1954, Dolomites in the Silurian and Devonian of east central Nevada: American Association Petroleum Geologists Bulletin, v. 38, p. 1911–56.

Potter, R. W., II, Clynne, M. A., and Brown, D. L., 1978, Freezing point depression of aqueous sodium chloride solutions: Economic Geology, v. 73, p. 284–85.

Radtke, A. S., 1985, Geology of the Carlin gold deposit, Nevada: U.S. Geological Survey Professional Paper 1267, 120p.

Radtke, A. S., and Dickson, F. W., 1974, Controls on the vertical position of fine-grained replacement-type gold deposits: International Association on the Genesis of Ore Deposits Symposium, 4th, Varna, Bulgaria, Abstracts, p. 68–69.

Radtke, A. S., Rye, R. O., and Dickson, F. W., 1980, Geology and stable isotope studies of the Carlin gold deposit, Nevada: Economic Geology, v. 75, p. 641–72.

Roedder, E., 1984, Fluid inclusions: Reviews in Mineralogy, v. 12, 644p.

Romberger, S. B., 1986, Ore deposits #9, Disseminated gold deposits: Geoscience Canada, v. 13, p. 23–31.

Seedorff, E., 1991, Magmatism, extension, and ore deposits of Eocene to Holocene age in the Great Basin—Mutual effects and preliminary

proposed genetic relationships: In Raines, G. L., Lisle, R. E., Schafer, R. W., and Wilkinson, W. H. (eds.), Geology and ore deposits of the Great Basin: Geological Society of Nevada, p. 133–78.

Sillitoe, R. H., and Bonham, H. F., Jr., 1990, Sediment-hosted gold deposits: Distal products of magmatic-hydrothermal systems: Geology, v. 18, p. 157–61.

Smith, D. L., Gans, P. B., and Miller, E. L., 1991, Palinspastic restoration of Cenozoic extension in the central and eastern Basin and Range province at latitude 39–40°N: In Raines, G. L., Lisle, R. E., Schafer, R. W., and Wilkinson, W. H. (eds.), Geology and ore deposits of the Great Basin: Geological Society of Nevada, p. 75–86.

Smith, R. M., 1976, Geology and mineral resources of White Pine County, Nevada, Part 2: Nevada Bureau of Mines and Geology Bulletin 85, p. 36–99.

Statistical Analysis Systems, 1988, SAS release 6.03: SAS Institute Inc., Cary, NC.

Stewart, J. H., 1980, Geology of Nevada: Nevada Bureau of Mines and Geology Special Publication 4, 136p.

Taylor, S. R., and McClennan, S. M., 1985, The continental crust: Its composition and evolution: Blackwell Scientific Publications, Oxford, 312p.

Theodore, T. G., and Jones, G. M., 1992, Geochemistry and geology of gold in jasperoid, Elephant Head area, Lander County, Nevada: U.S. Geological Survey Bulletin 2009, 53p.

Thorman, C. H., Ketner, K. B., Brooks, W. E., Snee, L. W., Zimmermann, R. A., 1991, Late Mesozoic–Cenozoic tectonics in northeastern Nevada: In Raines, G. L., Lisle, R. E., Schafer, R. W., and Wilkinson, W. H. (eds.), Geology and ore deposits of the Great Basin: Geological Society of Nevada, p. 25–45.

Tooker, E. W., 1985, Discussion of the disseminated-gold-ore-occurrence model: In Tooker, E. W. (ed.), Geologic characteristics of sediment- and volcanic-hosted disseminated gold deposits—Search for an occurrence model: U.S. Geological Survey Bulletin 1646, p. 107–50.

Welsh, J. E., and Miller, R. D., 1990, Butte Valley porphyry system, White Pine County, Nevada: Geology and ore deposits of the Great Basin, Reno/Sparks, Program with Abstracts, p. 113.

Wilson, D. J., 1992, Geology and geochemistry of the Golden Butte disseminated gold deposit, east central Nevada: M. S. thesis, Brigham Young University, 92p.

Wilson, W. R., Cox, J. W., and Lance, D. L., 1991, Geology and geochemistry of the Green Springs gold mine, White Pine County, Nevada: In Raines, G. L., Lisle, R. E., Schafer, R. W., and Wilkinson, W. H. (eds.), Geology and ore deposits of the Great Basin: Geological Society of Nevada, p. 687–700.

Wood, S. A., Crerar, D. A., and Borcsik, M. P., 1987, Solubility of the assemblage pyrite-pyrrhotite-magnetite-sphalerite-galena-gold-stibnite-bismuthinite-argentite-molybdenite in $H_2O$-NaCl-$CO_2$ solutions from 200° to 350° C: Economic Geology, v. 82, p. 1864–87.